

**Title: Erythroid differentiation in mouse erythroleukemia cells depends on Tmod3-mediated regulation of actin filament assembly into the erythroblast membrane skeleton**

**Running title:** Tmod3 promotes erythroid differentiation in Mel cells

Arit Ghosh<sup>1</sup>, Megan Coffin,<sup>1</sup> Richard West<sup>2</sup> and Velia M. Fowler<sup>1</sup>

**Affiliations:**

<sup>1</sup>Department of Biological Sciences, University of Delaware, Newark, DE, USA

<sup>2</sup>Delaware Biotechnology Institute, Newark DE, USA

**Corresponding author:**

Velia M. Fowler, Ph.D.  
Department of Biological Sciences  
University of Delaware  
105 The Green, 118 Wolf Hall  
Newark, DE 19716  
Tel: (302) 831-4296  
Fax: (302) 831-2281  
Email: [vfowler@udel.edu](mailto:vfowler@udel.edu)

**Abbreviations:** ED, erythroid differentiation; Tmod, tropomodulin; Tpm, tropomyosin; G-actin, globular (monomeric) actin; F-actin, filamentous actin; RBC, red blood cell; MEL ds19, mouse erythroleukemia clone ds19; KO, knockout; DMSO, dimethyl sulfoxide solution; HbA, Hemoglobin; CRISPR, clustered regularly interspaced short palindromic repeats; Cas9, CRISPR-associated protein 9; TMB 3,3',5,5'-tetramethylbenzidine; FACS, Fluorescence-activated cell sorting; 7-AAD, 7-aminoactinomycin D; SSC, side scatter; FSC, forward scatter; FITC, Fluorescein isothiocyanate; PE, phycoerythrin; APC, allophycocyanin; AF488, Alexa-Fluor 488.

**Acknowledgments:** We thank Dr. Yvette Yien for the gift of the Mel ds19 cell line. We also thank Dr. Kasturi Pal and Mr. Declan Cole for assistance in clonal selection of the Tmod3 knockout cells.

**Conflict of Interest statement:** “The authors have declared that no conflict of interest exists.”

**Author contributions:** A. Ghosh – performed and designed experiments, analyzed data, made figures, and wrote the paper. M. Coffin – performed experiments, analyzed data, made figures. R. West – designed experiments and analyzed data. V. M. Fowler – designed the research study and the experiments, wrote the paper.

**Funding:** This research was supported by a grant from the National Institute of Heart Lung and Blood at the National Institutes of Health (HL083464) to V.M.F.

### Abstract

Erythroid differentiation (ED) is a complex cellular process entailing morphologically distinct maturation stages of erythroblasts during terminal differentiation. Studies of actin filament (F-actin) assembly and organization during terminal ED have revealed essential roles for the F-actin pointed-end capping proteins, tropomodulins (Tmod1 and Tmod3). Tmods bind tropomyosins (Tpms), which enhance Tmod capping and F-actin stabilization. Tmods can also nucleate F-actin assembly, independent of Tpms. Tmod1 is present in the red blood cell (RBC) membrane skeleton, and deletion of *Tmod1* in mice leads to a mild compensated anemia due to mis-regulated F-actin lengths and membrane instability. Tmod3 is not present in RBCs, and global deletion of *Tmod3* leads to embryonic lethality in mice with impaired ED. To further decipher Tmod3's function during ED, we generated a *Tmod3* knockout in a mouse erythroleukemia cell line (Mel ds19). *Tmod3* knockout cells appeared normal prior to ED, but showed defects during progression of ED, characterized by a marked failure to reduce cell and nuclear size, reduced viability, and increased apoptosis. Tmod3 does not assemble with Tmod1 and Tpms into the Triton X-100 insoluble membrane skeleton during ED, and loss of Tmod3 had no effect on  $\alpha$ 1, $\beta$ 1-spectrin and protein 4.1R assembly into the membrane skeleton. However, F-actin, Tmod1 and Tpms failed to assemble into the membrane skeleton during ED in absence of Tmod3. We propose that Tmod3 nucleation of F-actin assembly promotes incorporation of Tmod1 and Tpms into membrane skeleton F-actin, and that this is integral to morphological maturation and cell survival during erythroid terminal differentiation.

**Keywords:** Erythrocyte membrane skeleton/ tropomodulin/ tropomyosin/ actin/ cell survival

## Introduction

Definitive erythropoiesis in mammals is characterized by the formation of mature red blood cells (RBCs) in the fetal liver and (postnatally) in the bone marrow via terminal differentiation and maturation of erythroid progenitors, accompanied by assembly of a membrane skeleton framework at the RBC membrane (1). Comprised of ~20 major proteins, the membrane skeleton is a two-dimensional periodic network of  $\alpha$ 1, $\beta$ 1-spectrin, short actin filaments (F-actin), band 4.1R, ankyrin and other actin-associated proteins (2). The membrane skeleton is critical for maintenance of RBC membrane deformability and stability, and thus cellular integrity, during microcirculation through the vasculature. Disruption of membrane skeleton components leads to hemolytic anemias in mice and humans, where RBCs are characterized by abnormal shapes, altered membrane deformability and stability (3, 4). Many hemolytic anemias arise from unstable interactions of spectrin or other network proteins with one another or with the membrane (5), while others may result from impaired membrane skeleton assembly during erythroid differentiation (ED), but this has been less well studied, and the mechanisms of membrane skeleton assembly are not well understood.

The temporal changes in membrane protein expression during ED have been well documented in a variety of systems including mice, chicken, and human RBCs (6, 7). Membrane skeleton proteins such as  $\alpha$ 1, $\beta$ 1-spectrin, 4.1R and ankyrin are synthesized early in differentiation but are only transiently and inefficiently assembled into the membrane skeleton, with a more stable assembly resulting upon subsequent expression of the anion transporter protein, band3 (6). On the other hand, actin expression decreases during ED (8), with the actin that persists reorganizing from the cytoplasmic cytoskeleton into the membrane skeleton in mature RBCs, which do not have a cytoplasmic cytoskeleton (2, 9). Correct F-actin assembly is

critical for RBC function, since perturbations in G:F (monomeric:filamentous) actin ratio in mature RBCs lead to abnormal membrane deformability in microfluidic assays (10). Notably, RhoGTPases Rac1 and Rac2 and associated signaling molecules that control actin polymerization and organization are vital for ED, and for correct assembly and maintenance of the RBC membrane skeleton (11, 12). Deletion of RBC membrane skeleton actin-binding proteins, such as dematin, tropomodulin1 (Tmod1) and tropomyosin (Tpm), also affect F-actin assembly into the membrane skeleton and contribute to RBC membrane instability (13-15). However, the mechanistic details of F-actin regulation in the context of dynamic cytoskeleton remodeling and membrane skeleton assembly during ED remains to be further investigated.

The actin capping proteins, tropomodulins (Tmods), are important players in membrane skeleton organization, ED, and enucleation. Tmods are a conserved family of proteins (Tmods1-4 in mammals) that regulate F-actin lengths and stability by capping the slow growing (pointed) filament ends and preventing F-actin assembly and disassembly (16, 17). Tmods' tight capping is promoted by their binding to tropomyosins (Tpms), which themselves bind along the length of F-actin, so that Tmods predominantly function to cap and stabilize the pointed ends of Tpm-coated F-actin in the cytoskeleton (18-20). Tmods can also bind actin monomers and nucleate F-actin assembly *in vitro*, which is independent of Tpms (21-23). However, a role for Tmods in F-actin nucleation in cells is not established (19, 20, 23).

Erythroid cells contain Tmod1 and Tmod3, with Tmod3 expressed early and decreasing during ED, while Tmod1 expression increases during mouse and human ED, similar to other membrane skeleton components, so that Tmod1 is the sole Tmod in mature RBCs (14, 24). While loss of Tmod1 has no effect on membrane skeleton protein expression or assembly during ED (14), RBCs from *Tmod1*<sup>-/-</sup> mice had a defective membrane skeleton with mis-regulated F-

actin lengths and an attenuated spectrin-F-actin lattice, resulting in membrane instability with a mild compensated hemolytic anemia (14). By contrast, a *Tmod3*<sup>-/-</sup> mouse is embryonic lethal at E14.5-E18.5 with evident anemia at E13.5 due to defective ED of fetal liver definitive erythroblasts with reduced survival, impaired cell cycle exit and reduced enucleation (24). The absence of *Tmod3* does not affect *Tmod1* expression, implying a unique *Tmod3* function during ED that *Tmod1* cannot replace. Moreover, enucleating *Tmod3*<sup>-/-</sup> fetal liver erythroblasts showed aberrant F-actin organization during enucleation (24). Mechanistically, it is not clear how lack of *Tmod3* leads to dysregulated ED, and whether *Tmod3* regulation of F-actin capping and stability is responsible.

Here, to directly assess the role of *Tmod3* in ED and membrane skeleton assembly we employed a murine erythroleukemia cell line (Mel ds19), which has been widely used to investigate many erythroid processes, including ED and membrane skeleton assembly, and is amenable to efficient and rapid genetic manipulation (25). We generated a *Tmod3* knockout Mel cell line using CRISPR-Cas9 technology and compared ED induced by DMSO in the parental Mel ds19 cells with *Tmod3*-knockout Mel cells. We utilized standard Triton X-100 based extraction and centrifugation to separate soluble and insoluble fractions to empirically assess membrane skeleton assembly in these cells (26). Our results demonstrate that lack of *Tmod3* leads to impaired ED with reduced cell survival and increased apoptosis, along with defective assembly of F-actin, *Tmod1* and *Tpms* into the Triton X-100 insoluble membrane skeleton. On the other hand,  $\alpha$ 1, $\beta$ 1-spectrin and protein 4.1R assembly into the membrane skeleton was unaffected in absence of *Tmod3*, indicating that neither F-actin, *Tmod1* nor *Tpms* are required to assemble a core membrane skeleton comprised of  $\alpha$ 1, $\beta$ 1-spectrin and protein 4.1R. Since *Tmod3* does not associate significantly with *Tpm*-coated F-actin prior to or during ED, we propose that

Tmod3 promotes F-actin nucleation for assembly with Tmod1 and Tpms into the membrane skeleton during ED. Our data also indicates that assembly of the membrane skeleton components,  $\alpha$ 1, $\beta$ 1-spectrin and protein 4.1R, is not sufficient to sustain normal ED, which requires concurrent assembly of Tmod1-Tpm-F-actin complexes.

## Materials and Methods

### Cell culture and erythroid differentiation

Mouse erythroleukemia (Mel) cell line clone ds19 (gift from Dr. Yvette Yien, University of Delaware) were cultured at 37°C (5% CO<sub>2</sub>) in suspension in DMEM media (#10-013-CV), containing 5% fetal bovine serum and 100 IU penicillin, 50 µg/ml streptomycin as described (27). To induce ED, exponentially growing Mel ds19 cells were seeded at a density of 2 x10<sup>5</sup> cells/ml and grown in media supplemented with 2% DMSO for 3 to 5 days (27).

### Generation of *Tmod3* knockout in Mel cells via CRISPR-Cas9

Using the CHOPCHOP web server (<http://chopchop.cbu.uib.no/>), three different guide RNAs were designed targeting exon 9b (sgRNA1), exon 9a (sgRNA2) and exon 9b (sgRNA3) of the *Tmod3* gene (Primers top/bottom: Table 1). The sgRNA oligo was generated using a primer annealing reaction (sgRNA top 10 µM, sgRNA bottom 10 µM, 1X T4 ligation buffer, 1U T4 PNK) via polynucleotide kinase (PNK) phosphorylation and an annealing program (37°C 30 min, 95°C 5 min; ramp down to 25°C at 5°C per min) as previously described (28). Annealed oligos (diluted 1:200) were cloned into pSp-Cas9(BB)-2A-GFP in a 20 µl reaction – (0.5 µl Cas9-GFP plasmid, 2 µl diluted oligo duplex, 2 µl 10X BbsI buffer, 1 µl 10 mM DTT, 1 µl 10 mM ATP, 1 µl BbsI, 0.5 µl T4 ligase, 12 µl ddH<sub>2</sub>O) using a thermocycler (Biorad T100<sup>TM</sup>) with cycles 1-6 (37°C for 5 min, 21°C for 5 min). The resulting product was transformed into DH5α competent cells and propagated for plasmid purification using a Qiagen Midiprep kit.

The purified plasmid – pSp-sgRNax-Cas9(BB)-2A-GFP was electroporated into Mel ds19 cells as previously described (29) with modifications. Cells were washed twice in 1X PBS and resuspended in DMEM (without FBS or antibiotic) and made up to 4x10<sup>6</sup> cells in 200 µl. 4

$\mu\text{l}$  of 1.5 M NaCl (tissue culture filtered) was added to 200  $\mu\text{l}$  of cells along with 20  $\mu\text{g}$  of the sgTMOD3-Cas9-GFP plasmid (or control plasmid lacking GFP). Cells were transferred to a chilled cuvette (0.4 cm Biorad, #165-2088) and pulse discharged using a setting of 280 V and 975  $\mu\text{F}$ . The cells were transferred to a 10  $\text{cm}^2$  plate and grown in 10 ml of DMEM (with 5% FBS, 1x Pen/Strep) for 48 hrs after which dead cells were stained with 7AAD (0.05  $\mu\text{g}/\text{ml}$ ), subjected to flow cytometry in a FACSAria Fusion flow cytometer, and live cells were gated and sorted for GFP expression (Supplemental Figure 1A). GFP positive cells were sorted into 96 well plates containing tissue culture filtered spent DMEM media and proliferating colonies were progressively transferred from 48- to 24- to 12- well plates depending on growth. Of the three guide RNAs, only sgRNA2 transfection led to viable colonies while the other two guides did not. Several clones (60 from sgRNA2) were screened individually (via western analyses) for the loss of Tmod3 protein. Clone #57 (data not shown) which lacked the Tmod3 protein band of interest was subsequently passaged five times and reanalyzed for the loss of Cas9-GFP from the population with the same gating strategies. Reassessment of Tmod3 protein loss was confirmed via three antibodies specific for various regions of the Tmod3 protein (Figure 1).

To further confirm gene loss, PCR amplified genomic DNA from the selected Tmod3 knockout clone was analyzed for missing sequence information via comparison to unedited Mel ds19 samples (Supplementary Figure 1B). To analyze any possible off-target effects from sgRNA2 expression, the predicted off-target sites (Chromosome 5, genomic position: 24,699,170; Chromosome 6, genomic position: 144,820,385) were amplified via primers flanking the predicted region and sequenced for the unedited Mel ds19 and Tmod3 knockout cell clone (Supplemental Figure S2A). The PCR products were sequenced using similar flanking primers to analyze the predicted region of interest (Supplemental Figure S2B).

### **Cell viability and TMB assay**

Cell viability was assessed by Trypan Blue staining using a 1:1 v/v cell to stain ratio and quantified on a BioRad TC20 cell counter to obtain total and live cell counts. Equal numbers of viable cells ( $2 \times 10^5$ ) were used to carry out the TMB (3,3',5,5'-tetramethylbenzidine) assay for heme as per manufacturer's instructions (Pierce #34021). Absorbance was measured at OD 450 nm using a Promega Glomax plate reader.

### **Giemsa staining and cell morphology measurements**

Control (untreated), 3d and 5d DMSO treated cells were used for Standard Giemsa staining.  $1 \times 10^5$  cells were cytopun (1,400 rpm for 3 mins at room temperature; Thermo Cytospin 4) onto glass slides and placed in 100% methanol for 5 mins for fixation. After air drying, the slides were immersed in Giemsa stain (Sigma-Aldrich, GS500) (1:10 diluted in deionized water), and stained for 1 hr. Post-staining, the slides were rinsed in deionized water to remove excess stain and air dried. Slides were examined on a Zeiss AxioImager A2 using a 63X objective lens (numerical aperture, N.A., 1.4) and images acquired with a color camera AxioCam 208, mono camera AxioCam 305 and processed using ZEN 3.0 software. Images from Giemsa staining of control, 3d and 5d cells (Mel ds19 and *Tmod3* KO) were used to measure cell and nuclear areas with the ImageJ freehand selection tool. For each measurement, N=30 cells were selected from each condition and respective cell line. Average cell or nuclear area is represented as a horizontal line on dot plots showing all data points. Experiments were carried out in triplicate.

## Flow Cytometry

All cell-based assays for flow cytometric analyses utilized cells initially seeded at  $2 \times 10^5$  cells/ml treated with or without 2% DMSO (for differentiation). All experiments were conducted in triplicate and analyzed using FCS Express 7 (Research edition DeNovo Software LLC).

*Annexin V-7AAD staining* – Cells from each condition were centrifuged at 2000 rpm, 2 mins at 4°C, washed with 1X PBS (with 1 mM EDTA) and stained with 5µl Annexin V conjugate in Annexin-binding buffer (30) (Table S2) along with 10µl 7-AAD (dead cell stain) in a final volume of 100µl. The suspension was incubated at room temperature for 15 mins, spun down at 1000 rpm for 3 mins to remove excess stain and resuspended in 500µl of Annexin-binding buffer. Unstained cells were used for gating controls and samples were acquired on a BD FACSAria™ Fusion flow cytometer.

*Cell Event Caspase 3/7 Green detection assay* – The CellEvent™ green detection reagent (Thermo #C10423) was used for detection of caspase3/7 activation according to the manufacturer's instructions. Cells were harvested and washed as mentioned above, and caspase 3/7 was detected on a BD Accuri C6 flow cytometer in the FITC channel (excitation/emission = 503/530m). Representative flow cytometry panels for percent of populations which are FITC positive [and 7AAD negative (live cells); data not shown] are shown in Figure S6B. The percent of the FITC positive population from each cell line was plotted on a bar graph (Figure 3C) as the mean  $\pm$  SD for 3d and 5d of growth in DMSO. An unstained sample (Mel ds19) was used as a negative gating control.

*CD71 trafficking* – For determination of surface and internal protein levels, a previously described method was adapted (31) with an Fc antibody (for blocking), CD71 PE (for surface)

and CD71 APC (for intracellular). Using the Fix and Perm method (Thermo #GAS003) we were able to detect surface CD71 levels (Figure S3) in the PE channel and internal CD71 levels in the APC channel (post-fixation and permeabilization). Cells were harvested and washed as above. Analyses were carried out on a BD Accuri C6 flow cytometer with appropriate color compensation and unstained controls.

*Propidium iodide staining and cell cycle analysis* – Cell cycle analysis was carried out via Propidium Iodide (PI) staining (control, 3d and 5d) and analyzed on a FACS Aria Fusion flow cytometer. Propidium Iodide (Sigma-Aldrich) (1mg/ml) was prepared in a modified Vindelov buffer (32) [5ml of stock 1mg/ml PI added to 95ml Tris-NaCl (1mM Tris, 1mM NaCl) buffered saline pH 8.0, 70U Ribonuclease A (Sigma-Aldrich), and 0.1 ml IGEPAL CA-630 (Sigma-Aldrich)]. Cells were resuspended in 500µl of PI staining solution and incubated at 4°C for 10 min before analysis. Multicycle analysis on FCS Express 7 software (33) was used to determine diploid G<sub>0</sub>/G<sub>1</sub>, diploid S, diploid G<sub>2</sub>/M phases count vs PE-A (PI stain) histograms (Figure S7).

*Isotype controls for surface CD71 PE and cytoplasmic CD71 APC* – Isotype controls were carried out for CD71 PE surface and cytoplasmic CD71 APC with PE Rat IgG1 (*k* isotype control) and APC Rat IgG2a (*k* isotype control) antibodies respectively. Mel ds19 cells (2 x 10<sup>5</sup> cells) were grown with or without 2% DMSO for 5 days and analyzed as follows: Set 1 – control and DMSO treated (unstained, stained with isotype control PE, stained with CD71 PE surface) and Set 2 – control and DMSO treated (fixed and permeabilized unstained, fixed and permeabilized isotype control PE & APC, fixed and permeabilized CD71 PE surface & CD71 APC). Cells were analyzed using FACS Aria Fusion flow cytometer with appropriate color compensation (Supplemental Figure S4A). Histograms for comparison of PE and APC

antibodies to isotype controls were made using FCS Express 7 software (Supplemental Figure S4B).

### **Total lysates and western blotting**

Total lysates for western blotting were obtained from control, 3d and 5d DMSO samples. Cell pellets ( $2 \times 10^6$  cells) were incubated in 50  $\mu$ l of extraction buffer [50 mM Tris-Cl pH 7.4, 150 mM NaCl, 1 mM EDTA, 1.5 mM  $MgCl_2$ , 1% Triton X-100, 1X protease inhibitor cocktail, 1X phosphatase inhibitor (ThermoFisher, Waltham, MA)] for 15 min on ice before sonicating for 10s on ice and centrifuging at 15,000 rpm for 15 mins at 4°C. Protein amount per sample was determined via BCA analysis using BSA as standard (ThermoFisher, Waltham, MA). For total lysates, equal amounts of protein (30  $\mu$ g) were loaded per lane. For western analyses all samples were electrophoresed on 4-12% SDS (Tris-Glycine) gels (ThermoFisher, Waltham, MA), except for the HbA blot which used 4-20% gels to detect the lower MW (~18 kDA) band for hemoglobin A. Proteins were immunoblotted to PVDF membranes (Millipore Sigma) using the semi-dry transfer (Biorad Trans-Blot Turbo™ #1704150), according to manufacturer's instructions (LiCoR #926-11010). Total protein was stained by incubating the PVDF membrane in Revert (Li-CoR Biosciences) protein stain and detected in the 700 nm channel with a Biorad Chemidoc Imaging system, prior to antibody labeling. Blocking was conducted using the LiCoR recommended blocking buffer (LiCoR BioSciences#927-70001) and primary antibody incubation was carried out overnight at 4°C with constant shaking in a fresh volume of LiCoR blocking buffer. The following day the blots were washed 3 times with 1X TBST (20mM Tris, 137 mM NaCl, 0.1% Tween-20) and incubated with appropriate secondary antibodies (680RD or 800CW) for 1 hour at RT according to manufacturer's instructions

(<https://www.licor.com/bio/applications/quantitative-western-blots/resources>) and washed 3 times with 1X TBST before image acquisition. The secondary antibody signals were detected in the 680 nm or 800 nm channels using a Chemidoc. Please refer to Supplemental Table 1 for complete list of antibodies used in the study along with other reagents.

### **Custom Tmod3 antibody preparation**

For preparation of immunopurified Tmod3 antibodies, we utilized Genscript's (Piscataway, NJ) antibody manufacturing services. The N-terminal peptide (PFRKDLGDYKDLDE) and a C-terminal peptide (VRKRRIEGDHQ) in the Tmod3 protein sequence was used to generate chicken anti-Tmod3 polyclonal antibodies (Figure 1B). Individuals can contact Dr. Velia M. Fowler, University of Delaware, Newark for these antibodies.

### **Triton X-100 subcellular fractionation**

Membrane skeleton assembly during ED was evaluated by an established approach of cell extraction with Triton X-100, followed by centrifugation to separate soluble (cytoplasmic) from insoluble (membrane skeleton) fractions (26). Triton X-100 soluble (S) and insoluble (P) fractions were prepared as previously described with modifications (34, 35). Cells from control, 3d and 5d DMSO treatment were spun down at 600g for 10 min at 4°C and washed twice with 1X PBS to remove cell debris and excess media. Samples were extracted in a Triton X-100 containing buffer under F-actin stabilizing conditions [Buffer A: 0.1 M PIPES pH 6.9, 30% Glycerol, 5% DMSO, 2 mM MgCl<sub>2</sub>, 100 mM KCl, 1 mM EGTA, 1% Triton X-100, 1 mM ATP, 1X protease inhibitor cocktail (ThermoFisher, Waltham, MA)] for 10 min on ice and centrifuged

at 100,000 *g* for 45 mins at 4°C to pellet the membrane skeleton and polymerized F-actin. The Triton X-100 soluble (S) supernatant fraction was removed, containing unassembled G-actin and other cytosolic components. The Triton X-100 insoluble pellet (P) containing the membrane skeleton and F-actin was resuspended by addition of an equivalent amount of an actin depolymerization buffer [Buffer B: 0.1 M PIPES pH 6.9, 2 mM MgCl<sub>2</sub>, 100 mM CaCl<sub>2</sub>, 1X protease inhibitor cocktail, 5 μM Cytochalasin D (ThermoFisher, Waltham, MA)], incubated for 30 min on ice and then sonicated for 10s to completely disperse and resuspend the pellet. The S and P samples were solubilized by addition of an equal volume of 2X Laemmli SDS-PAGE sample buffer (Biorad) and boiling for 5 min. Equal volumes of each (S and P) sample were loaded on 4-12% SDS-PAGE gels, and western analysis was conducted as above.

### **Western blot quantification**

*Western blot (total protein) analyses* – Band intensity was calculated using ImageJ and normalized to Total-Protein Revert™ staining before antibody labeling. Total protein lanes as detected from Revert™ staining were quantified to estimate the standard protein for normalization for each western blot. For each quantification, total area under the curve from image quantification was converted into percent using gel analysis options tool in ImageJ as described (<http://www.navbo.info/DensitometricAnalysys-NIHimage.pdf>). The intensity for each protein band (western blot) were normalized to total protein values. The average of the arbitrary units as ratiometric values of percent protein (western blot) to percent protein (total protein) are shown as bar graphs in Fig 4A and Fig 6A.

*Western blot (S and P fraction) analyses* – Band intensities from the western analyses for respective fractions S or P, were measured as described above using ImageJ, and values for S

and P fractions were added to obtain total intensity for each band. The intensity of the S or P band was divided by the total S+P, to obtain the percent soluble or in the pellet. Values were presented as an average  $\pm$  SD (N=3) for each timepoint (control, 3d and 5d) for the respective cell lines.

### **Statistical analysis.**

Data shown in dot plots and bar graphs are mean  $\pm$  standard deviation (SD). Differences between means were detected using Student's Paired T-tests. Statistical analysis was performed using GraphPad Prism 7.03 software. Statistical significance was defined as  $*p \leq 0.05$ ,  $**p \leq 0.01$ ,  $***p \leq 0.001$ ,  $****p \leq 0.0001$ .

## Results

### Generation of a *Tmod3* knockout in Mel cells

We showed previously that *Tmod3* is required for terminal differentiation of mouse fetal liver definitive erythroblasts *in vivo*, but whether this was a consequence of *Tmod3* regulation of F-actin in erythroblasts was not explored (24). To directly examine the role of *Tmod3* in ED, we adopted a CRISPR-Cas9 mediated knockout methodology to perturb the *Tmod3* gene in a mouse erythroleukemia cell line, Mel ds19 (25). We directed disruption of *Tmod3* gene exon 9b via a sgRNA-Cas9-GFP construct leading to a double-strand break followed by canonical non-homology end joining (NHEJ) directed repair (Figure 1A). The cells were sorted for GFP-Cas9 expression and viable clones were expanded and screened for loss of *Tmod3* via western blotting (Figure S1). To confirm the identity of the derived clone as a true *Tmod3* knockout we utilized antibodies detecting epitopes located in the N-terminal and C-terminal regions of *Tmod3* (custom-made antibodies) as well as a commercial antibody detecting an epitope in the middle region of the *Tmod3* protein (Supplemental Table 1, Materials and Methods). Lack of *Tmod3* in the selected clone confirmed that our clone of interest was a bonafide *Tmod3* knockout cell line (Figure 1B). The removal of Cas9-GFP was also tested in the selected clone via passaging and retesting for GFP expression using flow cytometry (Figure S1). Potential off-target effects due to sgRNA expression were ruled out by sequencing analysis and comparison of predicted off-target binding sites in unedited Mel ds19 and *Tmod3* knockout cells, which were unchanged (Figure S2).

### Lack of *Tmod3* leads to impaired Mel cell differentiation

To characterize the effects of *Tmod3* gene deletion, we analyzed cell viability (using trypan blue staining) during differentiation induced by growth in media containing 2% DMSO. The Mel ds19 control cell viability was high, with 88-90% live cells after 5d in DMSO, with a cell concentration of  $\sim 6 \times 10^6$  cells/ml. In contrast, the *Tmod3* KO cells had a significant decrease in viability ( $\sim 65\%$  live cells) after 5d in DMSO with a total cell count of  $\sim 2.5 \times 10^6$  cells/ml (Figure 2A). To assess the efficacy of DMSO induction of *in vitro* ED we investigated total hemoglobin production via a chromogenic assay utilizing TMB (3,3',5,5'-tetramethylbenzidine) as the substrate. As expected, DMSO treated Mel ds19 cells showed a 2-fold increase in TMB signal by 3d, which was sustained at day 5, signifying accumulation of hemoglobin during ED. While the *Tmod3* knockout cells showed an increase in hemoglobin signal at 3d, there was a significant decrease at 5d compared to the control Mel ds19 cells, suggesting lack of sustained expression of hemoglobin during ED in absence of *Tmod3* (Figure 2B). When we looked at surface and internal transferrin receptor (CD71) levels, we found that *Tmod3* KO cells showed CD71 expression patterns similar to control Mel ds19 cells (Figure S3, S4), indicating that *Tmod3* KO cells had normal features of ED even as overall differentiation was impaired.

We performed Wright-Giemsa staining to visualize morphological changes in the differentiating cells at 3d and 5d DMSO (Figure 2C). As control Mel ds19 cells differentiate, they show a gradual decrease in both cell and nuclear area, from 0d to 3d to 5d of DMSO treatment, as expected (Figure 2C-D) (36). The ratio of cell to nuclear area was unchanged from 0d to 3d to 5d, indicating that cell and nuclear areas decrease coordinately during ED (Figure S5). Before differentiation, the cells display a deep blue cytoplasm and a prominent nucleus. After 3d the cells are smaller with a reduced cytoplasmic area and lighter colored cytoplasm similar to polychromatic erythroblasts (Figures 2C-D). At 5d, the cell and nuclear area of the

control Mel ds19 cells decreased further (Figure 2C-D). While *Tmod3* KO cells resembled Mel ds19 cells in appearance with decreased cell and nuclear area after 3d, suggesting initial progression of ED, the KO cells failed to show any further cell and nuclear area decreases at 5d. Instead, the sizes of the 5d KO cells were increased compared to 3d KO cells, with a considerably larger cell (~2.5 fold) and nuclear (~3 fold) area as compared to 5d Mel ds19 cells (Figure 2D). Similar to control cells, the ratio of cell to nuclear area in was not different from 0d to 3d to 5d, indicating that changes in cell and nuclear area sizes are also coordinated in *Tmod3* KO cells (Figure S5). Such a pattern of initial morphological differentiation in *Tmod3* KO cells followed by partial reversal, is reminiscent of a similar trend for total hemoglobin production which increased at 3d but reversed and decreased at 5d for the KO, as shown above (TMB assay, Figure 2B). This suggests a temporal role for *Tmod3* protein in the later stages of terminal ED, and that *Tmod3* function is important for the transition from basophilic to polychromatic erythroblast.

### **Apoptosis is elevated in absence of *Tmod3* during ED**

Since a major decrease in viability was observed for *Tmod3* KO Mel cells during ED, we next looked for changes in apoptosis in the KO cells compared to the parent ds19 cells. Using Annexin V (AV) as a readout for apoptosis and 7AAD as a stain for dead cells, we looked at live, necrotic, early, and late apoptotic populations during ED with flow cytometry (Figure 3A). During proliferation of undifferentiated cells in absence of DMSO, apoptotic populations were low for both parent Mel ds19 cells and *Tmod3* KO cells, with the latter having a ~3-fold lower late apoptotic population compared to parental cells, whereas early apoptotic populations showed no significant differences between the two cell lines (Figure 3A, 3B). At 3d of differentiation, the

*Tmod3* KO showed a significantly higher degree of early apoptotic cells (~30%, ~3.5 fold more) compared to Mel ds19, while late apoptotic populations were similar. At 5d, the *Tmod3* KO had an even greater proportion of both early (~28%) and late (~48%) apoptotic cell populations compared to Mel ds19 cells, in which only ~4% of cells were early and ~18% late apoptotic cells (Figure 3A, 3B).

Executioner caspases 3/7 are integral for proper ED, with increased caspase3/7 required during terminal differentiation (37). Therefore, to further assess the abnormal increase in apoptosis in the *Tmod3* KO cells, we conducted a caspase3/7 cleavage-dependent DEVD peptide-based (CellEvent™) assay via flow cytometry for undifferentiated (control), 3d and 5d timepoints (Figure 3C, Figure S6). This showed that caspase 3/7 activity is elevated during ED in both control and *Tmod3* KO cells, but that *Tmod3* KO cells (at 5d DMSO) had ~4-fold higher levels of activated caspases compared to Mel ds19 cells during ED (Figure 3C). Based on the observed increases in early and late apoptotic cell populations ( $AV^{\text{high}}7AAD^{\text{high}}$ ) in the *Tmod3* KO cells, it is possible that overactivation of caspases in *Tmod3* KO during ED precipitates cells towards cell death. Previous studies have shown that differentiating murine erythroid progenitor cells will withdraw from cell cycle and accumulate into G1 phase (38). When we investigated cell cycle parameters for 5d of ED, and found that both Mel ds19 and KO cells appeared similar and were arrested at the G1 stage (Figure S7). This suggests that increase in apoptosis and decrease in cell survival in the *Tmod3* KO at 5d is independent of G1-phase arrest and cell cycle progression during ED.

### **Loss of *Tmod3* reduces *Tmod1* and actin assembly into the membrane skeleton**

A hallmark of terminal ED is the increased expression of  $\alpha 1, \beta 1$ -spectrin, protein 4.1R, Tmod1, among other components, and their assembly into the spectrin-F-actin filament network of the membrane skeleton, despite a decrease in total actin levels (7). To examine whether loss of Tmod3 affected membrane skeleton protein levels and assembly in Mel cells, we measured total levels of  $\alpha 1, \beta 1$ -spectrin, protein 4.1R, Tmod1 and actin, and their assembly into the Triton-X-100 insoluble membrane skeleton during ED. Western analyses of total lysates (control, 3d and 5d) revealed that as differentiation proceeds control Mel ds19 cells show ~5 to 9-fold increases in total  $\alpha 1, \beta 1$ -spectrin, protein 4.1R and Tmod1 levels, similar to primary murine erythroblasts (7) while total actin levels remained the same, as did levels of Tmod3 (Figure 4A, 4B). Loss of Tmod3 did not affect the increase in  $\alpha 1, \beta 1$ -spectrin, protein 4.1R, Tmod1 or actin that took place upon ED. Hemoglobin levels (HbA) also increased during ED in Mel ds19 cells, but this was reduced in *Tmod3* KO cells (Figure 4), in agreement with the TMB assay shown above (Figure 2). Thus, protein expression of major membrane skeleton components appears normal despite the absence of Tmod3, with reduced HbA expression and impaired morphological ED and cell death shown above.

To examine whether membrane skeleton assembly was affected by loss of Tmod3, we carried out sub-cellular fractionation using Triton X-100 to obtain a soluble fraction and insoluble pellet containing the membrane skeleton and F-actin (Figure 5A). First, we investigated membrane skeleton assembly of actin,  $\alpha 1, \beta 1$ -spectrin, protein 4.1R and Tmod1 in the control Mel ds19 cell line containing Tmod3. In undifferentiated Mel ds19 cells, nearly ~70% of actin was in the soluble fraction, with the remaining ~30% in the Triton X-100 insoluble pellet fraction (Figure 5). Since the membrane skeleton proteins ( $\alpha 1, \beta 1$ -spectrin, protein 4.1R and Tmod1) are not substantially expressed before ED, the actin in the pellet from undifferentiated

cells likely corresponds to F-actin in the cytoplasmic cytoskeleton. Upon ED, an increased proportion of actin is present in the Triton X-100 insoluble pellet (~50%), consistent with F-actin assembly into the membrane skeleton. As expected, induction of ED led to greatly increased expression of  $\alpha$ 1, $\beta$ 1-spectrin, protein 4.1R and Tmod1, along with their enrichment in the Triton X-100-insoluble pellet, indicative of membrane skeleton assembly (Figure 5B) (26). The presence of  $\alpha$ 1, $\beta$ 1-spectrin in both soluble and insoluble fractions during ED is similar to previous studies showing that  $\alpha$ 1, $\beta$ -spectrin polypeptides accumulate in excess during differentiation (26, 39). By contrast, Tmod3 remained in the soluble fractions in undifferentiated Mel cells and at 5d ED (~80-90%), with only a small proportion associating with the insoluble fraction during ED (~5% in the insoluble fraction at 0d and ~10% at 5d of ED) (Figure 5B, C).

Loss of Tmod3 had an adverse effect on actin as well as Tmod1 assembly into the membrane skeleton during ED (Figure 5B, 5C). While undifferentiated KO cells showed a similar distribution of actin and Tmod1 in the soluble and insoluble fractions as compared to Mel ds19 cells, lack of Tmod3 during ED led to reduced proportion of both actin and Tmod1 in the insoluble fractions at 5d. During ED, the relative proportion of actin and Tmod1 in the insoluble fraction in the Tmod3 KO was ~4-5 fold lower than for the Mel ds19 cells. Even so, band 4.1R and  $\alpha$ 1, $\beta$ 1-spectrin showed normal assembly into the TX-100 insoluble membrane skeleton in the Tmod3 KO during ED, similar to the control Mel ds19 cells. This indicates that Tmod1 and actin assembly into the membrane skeleton depend upon Tmod3, while  $\alpha$ 1, $\beta$ 1-spectrin and protein 4.1R can assemble into the membrane skeleton via a Tmod3, actin and Tmod1-independent pathway.

### **Tropomyosin assembly during ED is dysregulated in absence of Tmod3**

Previous studies of Tmod3 function in cells have shown that loss of Tmod3 leads to disassembly of Tpm-coated F-actin networks (18-20, 23). Mouse and human RBCs contain two Tpm isoforms, Tpm1.9 and Tpm3.1, that are associated with the short F-actin in the membrane skeleton (15). To determine which Tpm proteins were expressed in Mel ds19 and *Tmod3* KO Mel cells, we used a series of antibodies specific for exon  $\alpha$ -9d (Tpm1), exon  $\gamma$ -9d (Tpm3.1), and exon  $\delta$ -9d (Tpm4) to screen Mel ds19 cell extracts (Figure S8) (40). Based on these results, we selected two Tpm proteins, Tpm1 ( $\alpha$ -9d) and Tpm 3.1 ( $\gamma$ -9d, 5NM1), for further study during ED. Similar to actin and Tmod3 (Figure 4), Tpm1 and Tpm3.1/5NM1 levels do not increase in control Mel ds19 cells during ED (Figure 6A). This is unlike Tmod1, protein 4.1R and  $\alpha$ 1, $\beta$ 1-spectrin, whose levels increase significantly during ED (Figure 4). However, in *Tmod3* KO cells, levels of both Tpm1 and Tpm3.1 decreased significantly during ED, by about 50% and 60%, respectively (Figure 6A, B), again unlike Tmod1, protein 4.1R and  $\alpha$ 1, $\beta$ 1-spectrin whose expression levels increased even in the absence of Tmod3 (Figure 4).

To assess Tpm assembly with F-actin into the membrane skeleton during ED, we examined the proportion of Tpm proteins in the Triton X-100 soluble and insoluble fractions (41) (Figure 6C, D). In Mel ds19 undifferentiated cells, Tpm1 was preferentially associated with the insoluble fraction, a distribution which maintained during differentiation, while Tpm3.1 was enriched in the soluble as compared to the insoluble fraction (~2-fold greater) in undifferentiated cells, redistributing to a ~1:1 ratio during ED (Figure 6C, 6D). In contrast, in undifferentiated *Tmod3* KO cells, Tpm1 was evenly distributed between soluble and insoluble fractions, and upon differentiation did not associate with the insoluble fraction, remaining >4-fold higher in the soluble compared to insoluble fractions during ED. In undifferentiated *Tmod3* KO cells, Tpm3.1 was ~4-fold higher in soluble compared to insoluble fractions and ~10-fold higher in soluble

fractions after ED. Thus, similar to actin and Tmod1, loss of Tmod3 results in inability of these Tpm3s to assemble with  $\alpha$ 1, $\beta$ 1-spectrin and protein 4.1R into the membrane skeleton during ED.

## Discussion

In this study, we investigated the role of the pointed-end actin capping protein, Tmod3, in erythroid differentiation (ED) and F-actin assembly. Our results show that loss of Tmod3 in mouse erythroleukemia cells leads to impaired ED in Mel cells, based on decreased accumulation of hemoglobin, failure to reduce cell and nuclear size, reduced viability and increased apoptosis. These results parallel impaired ED observed for definitive ED in fetal liver of *Tmod3*<sup>-/-</sup> mice in our previous study (24). While *Tmod3*<sup>-/-</sup> fetal liver erythroid cells also exhibit impaired cell cycle exit, reduced enucleation frequency and abnormal F-actin during enucleation, parental Mel ds19 cells do not normally enucleate, and loss of Tmod3 does not affect cell cycle progression during ED in Mel cells. Thus, Tmod3's role in cell cycle exit in mouse fetal liver may be restricted to late stages of ED and/or be an indirect consequence of absence of Tmod3 in supporting cells such as macrophages (24). On the other hand, our results showing that loss of Tmod3 leads to impaired ED in Mel cells indicate a cell autonomous function for Tmod3 in ED prior to enucleation.

Tmod3 is required for correct F-actin assembly into the membrane skeleton during ED. *Tmod3*<sup>-/-</sup> Mel ds19 cells showed decreased assembly of Tmod1, Tpm3 and F-actin into the Triton-insoluble membrane skeleton during ED. However, unlike Tmod1 and Tpm3, Tmod3 is not a component of the RBC membrane skeleton (14), and is not significantly associated with the Triton X-100 insoluble membrane skeleton during normal ED in Mel ds19 cells. Tmod3 is also not associated with Tpm3 and F-actin in the insoluble fraction prior to ED. These observations suggest two possibilities for Tmod3 function in ED. One idea is that Tmod3 may transiently assemble with Tpm-F-actin, but be replaced by Tmod1 as Tmod1 levels increase during ED, leading to assembly of Tmod1-Tpm-F-actin complexes into the membrane skeleton.

Alternatively, a possibility that we favor is that Tmod3 may not function to stabilize Tpm-coated F-actin in Mel cells, either prior to or during ED, unlike Tmod3 in other cell contexts (15, 16, 18-20, 23). Instead, Tmod3 could function in the Mel cell cytoplasm to nucleate assembly of F-actin destined for incorporation into the membrane skeleton. Reduced F-actin nucleation for the membrane skeleton during ED would be expected to result in fewer filaments, thus precluding subsequent recruitment of Tmod1 and Tpm3 to F-actin for correct membrane skeleton assembly as ED progresses. Prior to ED, since the proportion of F-actin in the pellet is not affected by loss of Tmod3, it is likely that other F-actin nucleating proteins operate to promote F-actin assembly into the cytoskeleton (42). Future studies to rescue the phenotype of Tmod3 KO Mel cells by expressing Tmod3 proteins with mutations in their F-actin nucleating or Tpm-binding sites will be necessary to test whether Tmod3 regulates ED via nucleation of F-actin assembly or via Tpm binding to F-actin (16, 21, 22).

We also observed reduced total levels of Tpm1/ $\alpha$ -9d and Tpm3.1/ $\gamma$ -9d (5NM1) in *Tmod3*<sup>-/-</sup> Mel ds19 cells upon ED, while total levels of actin, Tmod1,  $\alpha$ 1, $\beta$ 1-spectrin and protein 4.1R were unaffected. It is possible that insufficient levels of Tmod3-nucleated F-actin and reduced assembly of Tpm3 would result in more soluble Tpm3, followed by their degradation. This would be analogous to results from previous studies showing that spectrin subunits synthesized in excess and not assembled into the membrane skeleton are targeted for degradation (43, 44). Future studies of Tpm protein synthesis and turnover would be required to address these questions.

In contrast to a Tmod3 requirement for assembly of F-actin, Tmod1 and Tpm3 during ED, loss of Tmod3 does not preclude assembly of  $\alpha$ 1, $\beta$ 1-spectrin or protein 4.1R into the Triton-insoluble membrane skeleton. This suggests that  $\alpha$ 1, $\beta$ 1-spectrin and protein 4.1R assemble

independently of F-actin, likely binding to the membrane via ankyrin or protein 4.1R linkages to Band3 (45, 46). The non-coordinate assembly of protein 4.1R with respect to Tmod1, Tpms and F-actin is also evident in protein 4.1R-null mouse RBCs, in which the level of Tmod1 is unaffected, Tpm is increased, and actin is somewhat reduced (46). Future studies of membrane skeleton assembly in human erythroid cell cultures, or using a conditional Tmod3 KO mouse with an erythroid-specific Tmod3 deletion will be needed to further assess Tmod3 function in membrane skeleton assembly and ED.

In Mel ds19 cells, similar to primary mouse and human erythroblasts (24), Tmod1 expression increases dramatically during ED and shows a ~40% increased association with the Triton-insoluble fraction, whereas Tmod3 levels do not increase, nor does it assemble into the Triton-insoluble fraction during ED. It is likely that increased Tmod1 during ED competes with Tmod3 for binding to pointed ends of F-actin assembling into the membrane skeleton, precluding association of Tmod3. This is supported by appearance of Tmod3 in *Tmod1*<sup>-/-</sup> mouse RBCs, with Tmod3 now associated with the membrane skeleton (14). Thus, Tmod3 is essential for Tmod1 assembly but not vice versa. Moreover, absence of Tmod1 does not affect ED, since *Tmod1*<sup>-/-</sup> mice have a mild compensated spherocytic anemia with increased reticulocytosis (14) and normal distributions of differentiating erythroblasts in fetal liver and bone marrow (47). Thus, despite not being a component of the final membrane skeleton, Tmod3 has a critical function in assembly of a key subset of membrane skeletal proteins – Tmod1, Tpms and F-actin, potentially by nucleating F-actin assembly destined for the membrane skeleton as proposed above. Dysregulated F-actin assembly during ED in absence of Tmod3 may also explain the abnormal F-actin organization and impaired enucleation observed in *Tmod3*<sup>-/-</sup> fetal liver erythroblasts (24).

In addition to Tmod3, other actin regulatory proteins that are not components of the RBC membrane skeleton are also critical for ED. For example, lack of Rac1 and Rac2 in mice alters actin assembly in RBCs causing membrane skeleton disruption, microcytic anemia and reticulocytosis (12). Rac1/2 KO mouse RBC ghosts have increased levels of actin and adducin phosphorylation, but Tmod1, Tpm and other proteins are unaffected. Actin and adducin associations with the Triton-insoluble membrane skeleton are also reduced, while Tmod1 and Tpm are unaffected, suggesting Rac1/2 regulation of actin assembly during ED via a divergent pathway from that controlled by Tmod3, which affects Tmod1 and Tpm assembly (11, 12). Genetic deletion of mouse Hem-1, a WAVE complex member which activates Arp2/3 in hematopoietic cells, leads to abnormal RBC shapes and aberrant F-actin foci in *Hem-1*<sup>-/-</sup> mouse RBCs (48). Additionally, *Hem-1*<sup>-/-</sup> RBC ghosts display reduced levels of membrane skeletal proteins such as  $\alpha$ 1, $\beta$ 1-spectrin, adducin, dematin, ankyrin, Band3, Band4.1R, and Tmod1, as well as increased adducin phosphorylation. This suggests an important role for actin regulation during ED by proteins that do not become part of the final membrane skeleton, as we report here for Tmod3 in Mel ds19 cells.

Our studies in Mel cells here, and in fetal liver erythroblasts (24) have both shown that loss of Tmod3 leads to reduced survival due to elevated apoptosis with increase in caspase3/7 activity. How does the erythroid cell relay the signals from identification of a destabilized membrane to cellular machineries that result in apoptosis? Several studies have demonstrated a role for the actin cytoskeleton as a trigger for apoptosis (49). Treatment of HeLa cells with cytochalasin B (inhibitor of actin polymerization) leads to caspase-mediated cytochrome c release indicative of actin-dependent mitochondrial membrane de-stability (50). Gelsolin (barbed end F-actin binding protein) can induce apoptosis by dissociating the G-actin:DNAase I

complex, leading to nuclear localization and activation of DNase I (51). Bcl-2 proteins have also been shown to have a direct link to actin-mediated apoptosis as the pro-survival Bcl-X<sub>L</sub> protein suppresses apoptosis induced via cytochalasin D in Jurkat cells (52). One can speculate that loss of an F-actin capping and nucleating protein such as Tmod3 with reduced F-actin assembly and/or stability might act as a trigger activation of signaling cascades leading to abrogation of increase in Bcl-X<sub>L</sub> expression, culminating in erythroid cell death. Alternatively, or additionally, the lack of Tmod3 leading to an atypical erythroid membrane skeleton network (with no Tmod1, Tpm5 or F-actin) could lead to aberrant membrane receptor signaling pathways, reduced cell survival and increased cell death. Further studies to elucidate Tmod3's binding partners and signaling pathways in erythroblasts will be necessary to elucidate the mechanistic connections between Tmod3 regulation of actin assembly with cell survival and progression of ED.

**Acknowledgments:** We thank Dr. Yvette Yien for the gift of the Mel ds19 cell line. We also thank Dr. Kasturi Pal and Mr. Declan Cole for assistance in clonal selection of the Tmod3 knockout cells.

**Conflict of Interest statement:** “The authors have declared that no conflict of interest exists.”

**Author contributions:** A. Ghosh – performed and designed experiments, analyzed the data, made the figures, and wrote the paper. M. Coffin – performed experiments, analyzed data, made figures R. West – designed experiments and analyzed the data. V. M. Fowler – designed the research study and the experiments, and wrote the paper.

**Data availability statement:** *Included in article* - The data that support the findings of this study are available in the methods and/or supplementary material of this article.

**References:**

1. Palis, J. (2014) Primitive and definitive erythropoiesis in mammals. *Front Physiol* **5**, 3
2. Fowler, V. M. (2013) The human erythrocyte plasma membrane: a Rosetta Stone for decoding membrane-cytoskeleton structure. *Curr Top Membr* **72**, 39-88
3. Mohandas, N., and Evans, E. (1994) Mechanical properties of the red cell membrane in relation to molecular structure and genetic defects. *Annu Rev Biophys Biomol Struct* **23**, 787-818
4. Da Costa, L., Galimand, J., Fenneteau, O., and Mohandas, N. (2013) Hereditary spherocytosis, elliptocytosis, and other red cell membrane disorders. *Blood Rev* **27**, 167-178
5. Andolfo, I., Russo, R., Gambale, A., and Iolascon, A. (2016) New insights on hereditary erythrocyte membrane defects. *Haematologica* **101**, 1284-1294
6. Lazarides, E., and Woods, C. (1989) Biogenesis of the red blood cell membrane-skeleton and the control of erythroid morphogenesis. *Annu Rev Cell Biol* **5**, 427-452
7. Chen, K., Liu, J., Heck, S., Chasis, J. A., An, X., and Mohandas, N. (2009) Resolving the distinct stages in erythroid differentiation based on dynamic changes in membrane protein expression during erythropoiesis. *Proc Natl Acad Sci U S A* **106**, 17413-17418
8. Wickrema, A., Koury, S. T., Dai, C. H., and Krantz, S. B. (1994) Changes in cytoskeletal proteins and their mRNAs during maturation of human erythroid progenitor cells. *J Cell Physiol* **160**, 417-426
9. Liu, J., Guo, X., Mohandas, N., Chasis, J. A., and An, X. (2010) Membrane remodeling during reticulocyte maturation. *Blood* **115**, 2021-2027
10. Gokhin, D. S., Nowak, R. B., Khoory, J. A., Piedra, A. e. L., Ghiran, I. C., and Fowler, V. M. (2015) Dynamic actin filaments control the mechanical behavior of the human red blood cell membrane. *Mol Biol Cell* **26**, 1699-1710
11. Konstantinidis, D. G., George, A., and Kalfa, T. A. (2010) Rac GTPases in erythroid biology. *Transfus Clin Biol* **17**, 126-130
12. Kalfa, T. A., Pushkaran, S., Mohandas, N., Hartwig, J. H., Fowler, V. M., Johnson, J. F., Joiner, C. H., Williams, D. A., and Zheng, Y. (2006) Rac GTPases regulate the morphology and deformability of the erythrocyte cytoskeleton. *Blood* **108**, 3637-3645
13. Lu, Y., Hanada, T., Fujiwara, Y., Nwankwo, J. O., Wieschhaus, A. J., Hartwig, J., Huang, S., Han, J., and Chishti, A. H. (2016) Gene disruption of dematin causes precipitous loss of erythrocyte membrane stability and severe hemolytic anemia. *Blood* **128**, 93-103
14. Moyer, J. D., Nowak, R. B., Kim, N. E., Larkin, S. K., Peters, L. L., Hartwig, J., Kuypers, F. A., and Fowler, V. M. (2010) Tropomodulin 1-null mice have a mild spherocytic elliptocytosis with appearance of tropomodulin 3 in red blood cells and disruption of the membrane skeleton. *Blood* **116**, 2590-2599
15. Sui, Z., Gokhin, D. S., Nowak, R. B., Guo, X., An, X., and Fowler, V. M. (2017) Stabilization of F-actin by tropomyosin isoforms regulates the morphology and mechanical behavior of red blood cells. *Mol Biol Cell* **28**, 2531-2542
16. Yamashiro, S., Gokhin, D. S., Kimura, S., Nowak, R. B., and Fowler, V. M. (2012) Tropomodulins: pointed-end capping proteins that regulate actin filament architecture in diverse cell types. *Cytoskeleton (Hoboken)* **69**, 337-370
17. Ghosh, A., and Fowler, V. M. (2021) Tropomodulins. *Curr Biol* **31**, R501-R503

18. Kumari, R., Jiu, Y., Carman, P. J., Tojkander, S., Kogan, K., Varjosalo, M., Gunning, P. W., Dominguez, R., and Lappalainen, P. (2020) Tropomodulins Control the Balance between Protrusive and Contractile Structures by Stabilizing Actin-Tropomyosin Filaments. *Curr Biol* **30**, 767-778.e765
19. Weber, K. L., Fischer, R. S., and Fowler, V. M. (2007) Tmod3 regulates polarized epithelial cell morphology. *J Cell Sci* **120**, 3625-3632
20. Gokhin, D. S., and Fowler, V. M. (2011) Cytoplasmic gamma-actin and tropomodulin isoforms link to the sarcoplasmic reticulum in skeletal muscle fibers. *J Cell Biol* **194**, 105-120
21. Yamashiro, S., Speicher, K. D., Speicher, D. W., and Fowler, V. M. (2010) Mammalian tropomodulins nucleate actin polymerization via their actin monomer binding and filament pointed end-capping activities. *J Biol Chem* **285**, 33265-33280
22. Yamashiro, S., Gokhin, D. S., Sui, Z., Bergeron, S. E., Rubenstein, P. A., and Fowler, V. M. (2014) Differential actin-regulatory activities of Tropomodulin1 and Tropomodulin3 with diverse tropomyosin and actin isoforms. *J Biol Chem* **289**, 11616-11629
23. Parreno, J., and Fowler, V. M. (2018) Multifunctional roles of tropomodulin-3 in regulating actin dynamics. *Biophys Rev* **10**, 1605-1615
24. Sui, Z., Nowak, R. B., Bacconi, A., Kim, N. E., Liu, H., Li, J., Wickrema, A., An, X. L., and Fowler, V. M. (2014) Tropomodulin3-null mice are embryonic lethal with anemia due to impaired erythroid terminal differentiation in the fetal liver. *Blood* **123**, 758-767
25. Yik, J. J., Crossley, M., and Quinlan, K. G. R. (2018) Genome Editing of Erythroid Cell Culture Model Systems. *Methods Mol Biol* **1698**, 245-257
26. Basu, A., Harper, S., Pesciotta, E. N., Speicher, K. D., Chakrabarti, A., and Speicher, D. W. (2015) Proteome analysis of the triton-insoluble erythrocyte membrane skeleton. *J Proteomics* **128**, 298-305
27. Yien, Y. Y., Ducamp, S., van der Vorm, L. N., Kardon, J. R., Manceau, H., Kannengiesser, C., Bergonia, H. A., Kafina, M. D., Karim, Z., Gouya, L., Baker, T. A., Puy, H., Phillips, J. D., Nicolas, G., and Paw, B. H. (2017) Mutation in human. *Proc Natl Acad Sci U S A* **114**, E8045-E8052
28. Ran, F. A., Hsu, P. D., Wright, J., Agarwala, V., Scott, D. A., and Zhang, F. (2013) Genome engineering using the CRISPR-Cas9 system. *Nat Protoc* **8**, 2281-2308
29. Bieker, J. J., and Southwood, C. M. (1995) The erythroid Krüppel-like factor transactivation domain is a critical component for cell-specific inducibility of a beta-globin promoter. *Mol Cell Biol* **15**, 852-860
30. Koopman, G., Reutelingsperger, C. P., Kuijten, G. A., Keehnen, R. M., Pals, S. T., and van Oers, M. H. (1994) Annexin V for flow cytometric detection of phosphatidylserine expression on B cells undergoing apoptosis. *Blood* **84**, 1415-1420
31. Eisenmann, K. M., West, R. A., Hildebrand, D., Kitchen, S. M., Peng, J., Sigler, R., Zhang, J., Siminovitch, K. A., and Alberts, A. S. (2007) T cell responses in mammalian diaphanous-related formin mDia1 knock-out mice. *J Biol Chem* **282**, 25152-25158
32. Vindelov, L. L. (1977) Flow microfluorometric analysis of nuclear DNA in cells from solid tumors and cell suspensions. A new method for rapid isolation and straining of nuclei. *Virchows Arch B Cell Pathol* **24**, 227-242
33. Rabinovitch, P. S. (1994) DNA content histogram and cell-cycle analysis. *Methods Cell Biol* **41**, 263-296

34. Pal, K., Nowak, R., Billington, N., Liu, R., Ghosh, A., Sellers, J. R., and Fowler, V. M. (2020) Megakaryocyte migration defects due to nonmuscle myosin IIA mutations underlie thrombocytopenia in MYH9-related disease. *Blood* **135**, 1887-1898
35. Smith, A. S., Pal, K., Nowak, R. B., Demenko, A., Zaninetti, C., Da Costa, L., Favier, R., Pecci, A., and Fowler, V. M. (2019) MYH9-related disease mutations cause abnormal red blood cell morphology through increased myosin-actin binding at the membrane. *Am J Hematol* **94**, 667-677
36. Friend, C., Scher, W., Holland, J. G., and Sato, T. (1971) Hemoglobin synthesis in murine virus-induced leukemic cells in vitro: stimulation of erythroid differentiation by dimethyl sulfoxide. *Proc Natl Acad Sci U S A* **68**, 378-382
37. Zhao, B., Mei, Y., Schipma, M. J., Roth, E. W., Bleher, R., Rappoport, J. Z., Wickrema, A., Yang, J., and Ji, P. (2016) Nuclear Condensation during Mouse Erythropoiesis Requires Caspase-3-Mediated Nuclear Opening. *Dev Cell* **36**, 498-510
38. Hsieh, F. F., Barnett, L. A., Green, W. F., Freedman, K., Matushansky, I., Skoultchi, A. I., and Kelley, L. L. (2000) Cell cycle exit during terminal erythroid differentiation is associated with accumulation of p27(Kip1) and inactivation of cdk2 kinase. *Blood* **96**, 2746-2754
39. Pfeffer, S. R., Huima, T., and Redman, C. M. (1986) Biosynthesis of spectrin and its assembly into the cytoskeletal system of Friend erythroleukemia cells. *J Cell Biol* **103**, 103-113
40. Schevzov, G., Whittaker, S. P., Fath, T., Lin, J. J., and Gunning, P. W. (2011) Tropomyosin isoforms and reagents. *Bioarchitecture* **1**, 135-164
41. Bryce, N. S., Schevzov, G., Ferguson, V., Percival, J. M., Lin, J. J., Matsumura, F., Bamberg, J. R., Jeffrey, P. L., Hardeman, E. C., Gunning, P., and Weinberger, R. P. (2003) Specification of actin filament function and molecular composition by tropomyosin isoforms. *Mol Biol Cell* **14**, 1002-1016
42. Gokhin, D. S., and Fowler, V. M. (2016) Feisty filaments: actin dynamics in the red blood cell membrane skeleton. *Curr Opin Hematol* **23**, 206-214
43. Ciana, A., Achilli, C., and Minetti, G. (2017) Spectrin and Other Membrane-Skeletal Components in Human Red Blood Cells of Different Age. *Cell Physiol Biochem* **42**, 1139-1152
44. Woods, C. M., and Lazarides, E. (1985) Degradation of unassembled alpha- and beta-spectrin by distinct intracellular pathways: regulation of spectrin topogenesis by beta-spectrin degradation. *Cell* **40**, 959-969
45. Mohandas, N., and Gallagher, P. G. (2008) Red cell membrane: past, present, and future. *Blood* **112**, 3939-3948
46. Salomao, M., Zhang, X., Yang, Y., Lee, S., Hartwig, J. H., Chasis, J. A., Mohandas, N., and An, X. (2008) Protein 4.1R-dependent multiprotein complex: new insights into the structural organization of the red blood cell membrane. *Proc Natl Acad Sci U S A* **105**, 8026-8031
47. Nowak, R. B., Papoin, J., Gokhin, D. S., Casu, C., Rivella, S., Lipton, J. M., Blanc, L., and Fowler, V. M. (2017) Tropomodulin 1 controls erythroblast enucleation via regulation of F-actin in the enucleosome. *Blood* **130**, 1144-1155
48. Chan, M. M., Wooden, J. M., Tsang, M., Gilligan, D. M., Hirehallur-S, D. K., Finney, G. L., Rynes, E., Maccoss, M., Ramirez, J. A., Park, H., and Iritani, B. M. (2013)

- Hematopoietic protein-1 regulates the actin membrane skeleton and membrane stability in murine erythrocytes. *PLoS One* **8**, e54902
49. Desouza, M., Gunning, P. W., and Stehn, J. R. (2012) The actin cytoskeleton as a sensor and mediator of apoptosis. *Bioarchitecture* **2**, 75-87
  50. Kulms, D., Düssmann, H., Pöppelmann, B., Ständer, S., Schwarz, A., and Schwarz, T. (2002) Apoptosis induced by disruption of the actin cytoskeleton is mediated via activation of CD95 (Fas/APO-1). *Cell Death Differ* **9**, 598-608
  51. Chhabra, D., Nosworthy, N. J., and dos Remedios, C. G. (2005) The N-terminal fragment of gelsolin inhibits the interaction of DNase I with isolated actin, but not with the cofilin-actin complex. *Proteomics* **5**, 3131-3136
  52. Celeste Morley, S., Sun, G. P., and Bierer, B. E. (2003) Inhibition of actin polymerization enhances commitment to and execution of apoptosis induced by withdrawal of trophic support. *J Cell Biochem* **88**, 1066-1076

## Figure Legends

**Figure 1. Generation of a *Tmod3* knockout mouse erythroleukemia cell line by CRISPR-Cas9.** (A) A *Tmod3* knockout line was created with CRISPR-Cas9 employing a one-plasmid system expressing a guide RNA and Cas9-GFP to target exon 9b on the *Tmod3* gene. Post-electroporation, the cells were sorted for GFP expression via flow cytometry and clones were expanded for screening via western blotting (Supplemental Figure S1). (B) Mouse *Tmod3* amino acid sequence with locations of peptides (red – Nterm, blue - Cterm) used to prepare custom chicken anti-*Tmod3* antibodies (Genscript). A commercial rabbit anti-*Tmod3* antibody (Aviva) raised against the middle region of *Tmod3* (pink) was used as well. These three different *Tmod3* antibodies detecting various epitopes (Nterm Ab, Mid Ab and Cterm Ab), were used to confirm *Tmod3* protein loss in the *Tmod3* knockout (KO) cells by western blot (upper panels). Total protein was detected using revert stain (LiCoR) (lower panels).

**Figure 2. *Tmod3* knockout leads to decreased cell viability, reduced hemoglobin and impaired erythroid differentiation.** (A) Mel ds19 and *Tmod3* KO cells were seeded at  $2 \times 10^5$  cells/ml and grown for 3-5 days in culture media supplemented with 2% DMSO to induce erythroid differentiation (ED). The control timepoint denotes undifferentiated cells after 5 days of culture without DMSO treatment. At each timepoint cells were stained with trypan blue to ascertain cell viability and the percentage of live cells was counted. (B) The TMB (3,3',5,5'-tetramethylbenzidine) assay was used to determine total hemoglobin content in Mel ds19 and *Tmod3* KO cell lines, using equal numbers ( $2 \times 10^5$ ) of live cells (trypan blue staining) for each time point (control (cnt), 3d and 5d). The graph represents an average of triplicates with a mean  $\pm$  S.D. (C) Wright-Giemsa staining was used to analyze morphological changes in the two cell

lines during ED. Representative images are shown for control, 3d and 5d DMSO conditions. Insets display a single cell from the main panel (indicated with an arrowhead) at a higher magnification to illustrate morphological differences between the two cell lines. Scale bar = 10  $\mu\text{m}$ . (D). Scatter plots representing mean cell and nuclear area for Mel ds19 and *Tmod3* KO cells were obtained from Giemsa staining (N=30 cells; data shown is representative of three independent experiments). Horizontal line on scatter plots represents average cell or nuclear area, with SD indicated. Cell Area ( $\mu\text{m}^2$ ) – Mel ds19 (control –  $316.6 \pm 71.6$ , 3d –  $218.3 \pm 45.7$ , 5d –  $114.6 \pm 15.9$ ), *Tmod3* KO (control –  $308.0 \pm 79.3$ , 3d –  $197.7 \pm 45.0$ , 5d –  $249.9 \pm 58.8$ ). Nuclear Area ( $\mu\text{M}$ ) – Mel ds19 (control –  $163.8 \pm 37.0$ , 3d –  $120.1 \pm 28.2$ , 5d –  $64.7 \pm 10.2$ ), *Tmod3* KO (control –  $159.4 \pm 36.6$ , 3d –  $113.5 \pm 24.6$ , 5d –  $136.1 \pm 37.2$ ). ns – not significant, \*\*  $p \leq 0.01$ , \*\*\*  $p \leq 0.001$ , \*\*\*\*  $p \leq 0.0001$ .

**Figure 3. Increased apoptosis during erythroid differentiation in *Tmod3* knockout cells.** (A) Annexin V and 7AAD staining in Mel ds19 and *Tmod3* knockout cells was conducted for control (undifferentiated), 3d DMSO and 5d DMSO conditions (differentiating cells). Representative flow cytometry density plots are shown for each timepoint and corresponding cell line. Quadrants denote: live (AnnexinV<sup>low</sup>7AAD<sup>low</sup>), necrotic (AnnexinV<sup>low</sup>7AAD<sup>high</sup>), early apoptotic (AnnexinV<sup>high</sup>7AAD<sup>low</sup>) and late apoptotic (AnnexinV<sup>high</sup>7AAD<sup>high</sup>) cells. (B) Bar graphs showing percentage of cells in early and late apoptotic populations for Mel ds19 and *Tmod3* knockout cells in control (undifferentiated), 3d and 5d DMSO (differentiating) conditions, from flow cytometry data as in A. Values are means  $\pm$  S.D. (n=3 experiments). \*  $p \leq 0.05$ . (C) Caspase 3/7 flow cytometry assays are shown for Mel ds19 and *Tmod3* knockout cells for 3d and 5d timepoints. Left panels, Representative histograms denote Caspase3/7 FITC fluorescence

intensities with Mel ds19 in gray and *Tmod3* KO in black. The vertical line on the plots demarcates the negative (C3/7-) and the positive caspase 3/7 signal (C3/7+), based on gating of unstained samples (Supplemental Figure S6A). Right panel, Bar graph showing caspase 3/7 positive cells, plotted as a percentage of total population (Caspase 3/7 FITC positive; derived from Supplemental Figure S6C) for control, 3d and 5d cells (Mel ds19 and *Tmod3* KO). Experiments were carried out in triplicate. ns – not significant. \*  $p \leq 0.05$ .

**Figure 4. Loss of *Tmod3* does not affect increases in levels of Band 4.1R,  $\alpha$ 1, $\beta$ 1-Spectrin, *Tmod1* and Hemoglobin A (HbA) during erythroid differentiation.** (A) Immunoblots of *Tmod3*, *Tmod1*, Band 4.1R,  $\alpha$ 1, $\beta$ 1-Spectrin, Actin and HbA in Mel ds19 and *Tmod3* knockout cells grown in absence of DMSO for 5d (control) or in presence of DMSO for 3d and 5d. Each lane was loaded with 30  $\mu$ g of total lysates from respective timepoints for each cell line and immunoblotted for proteins as indicated. Bottom panel, Total protein is shown as Revert<sup>TM</sup> 700 protein stain and used as a loading control. Representative immunoblots are shown. (B) Bar graphs showing relative levels of protein of interest, normalized to total protein, quantified from immunoblots, and denoted as arbitrary units on Y axes for comparison. Values represent means  $\pm$  SD (N=3 independent experiments). *Tmod1*, band 4.1R,  $\alpha$ 1, $\beta$ 1-Spectrin and HbA levels increase during ED in Mel ds19 and *Tmod3* KO cells, while *Tmod3* and actin levels remain constant. No *Tmod3* is detected in the KO cells. \*  $p \leq 0.05$ , \*\*  $p \leq 0.01$

**Figure 5. Loss of *Tmod3* leads to reduced assembly of actin and *Tmod1*, but not protein 4.1R or  $\alpha$ 1, $\beta$ 1-Spectrin, into the Triton-insoluble membrane skeleton during erythroid differentiation.** (A) Experimental workflow for protein fractionation into Triton X-100 soluble

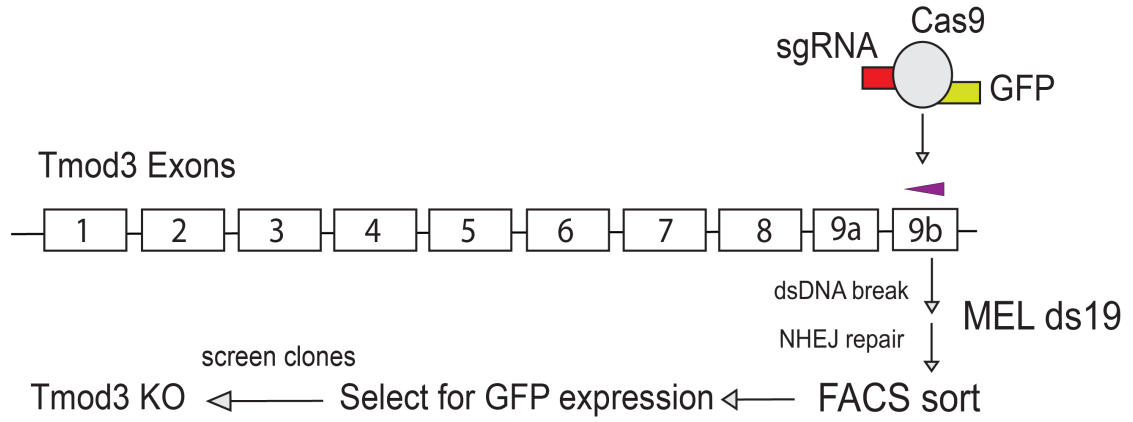
(S) and insoluble (P) fractions. Cells growing with or without DMSO were lysed in Triton X-100 based Buffer A and the supernatant was removed as the Triton X-100 soluble fraction (S) and the resulting pellet was resuspended in Buffer B (actin depolymerizing buffer) followed by solubilization for SDS gels. (B) Immunoblots of actin, band 4.1R,  $\alpha$ 1, $\beta$ 1-Spectrin, Tmod1 and Tmod3 in Triton X-100 soluble (S) and insoluble (P) fractions from Mel ds19 or *Tmod3* KO cells grown in the absence (-) or presence (+) of DMSO for 5d. Equivalent volumes of S and P fractions (10  $\mu$ l) were loaded in each lane (see Materials and Methods), and representative immunoblots are shown. (B) Bar graphs showing percent in S and P fractions expressed as a percentage of the total S+P. Values for percent of actin, Band4.1R,  $\alpha$ 1, $\beta$ 1-Spectrin, Tmod3 and Tmod1 in S and P fractions are shown as means  $\pm$  SD. Values represent N=3 independent experiments. ns – not significant, \*  $p \leq 0.05$ , \*\*  $p \leq 0.01$ , \*\*\*  $p \leq 0.001$ , \*\*\*\*  $p \leq 0.0001$ .

**Figure 6. Tropomyosin levels and assembly into the Triton-insoluble membrane skeleton are reduced during erythroid differentiation of *Tmod3* knockout cells.** (A) Immunoblots of tropomyosins, Tpm1/ $\alpha$ -9d and Tpm3.1/ $\gamma$ -9d (5NM1), in Mel ds19 and *Tmod3* KO cells during ED via immunoblotting. Total protein (Revert<sup>TM</sup> 700 stain, LiCor) was used as loading control. (B) Bar graphs showing relative levels of Tpms, normalized to total protein, quantified from blots as in A, denoted as arbitrary units on Y axes. Tpm1/ $\alpha$ -9d and Tpm3.1/ $\gamma$ -9d (5NM1) did not increase during ED in Mel ds19 cells, while loss of Tmod3 led to significant decreases in both Tpms during differentiation. (C) Immunoblots of Tpm1/ $\alpha$ -9d and Tpm3.1/ $\gamma$ -9d (5NM1) in Triton X-100 soluble (S) and insoluble (P) fractions from Mel ds19 and *Tmod3* knockout cells grown in the absence (-) or presence (+) of DMSO for 5d cells. Each lane was loaded with equivalent volumes of S and P (10  $\mu$ l), and representative immunoblots are shown. Total protein is shown

as Revert<sup>TM</sup> 700 staining (LiCoR). (D) Bar graph showing percents of Tpm1/ $\alpha$ -9d or Tpm3.1/ $\gamma$ -9d (5NM1) in S and P fractions expressed as a percentage of total S+P. In Mel ds19 cells, Tpm1/ $\alpha$ -9d levels consistently associate with P fractions in both control and differentiated cells, while Tpm3.1/ $\gamma$ -9d (5NM1) redistributes from S to P fraction as differentiation proceeds. Lack of Tmod3 led to complete loss of both Tpm1/ $\alpha$ -9d and Tpm3.1/ $\gamma$ -9d (5NM1) from the P fractions during differentiation. Values represent means  $\pm$  SD. N=3 independent experiments. ns – not significant, \*  $p \leq 0.05$ , \*\*  $p \leq 0.01$ , \*\*\*  $p \leq 0.001$ .

# Figure 1

**A.**



**B.**

Tmod3 (Nterm Ab) ▽

MALPFRKDLGDYKDLDEDELLGKLSESELKQLETVLDLDPENALLPAGFRQKNQTSK SAT Tmod3 (Mid Ab) ▽

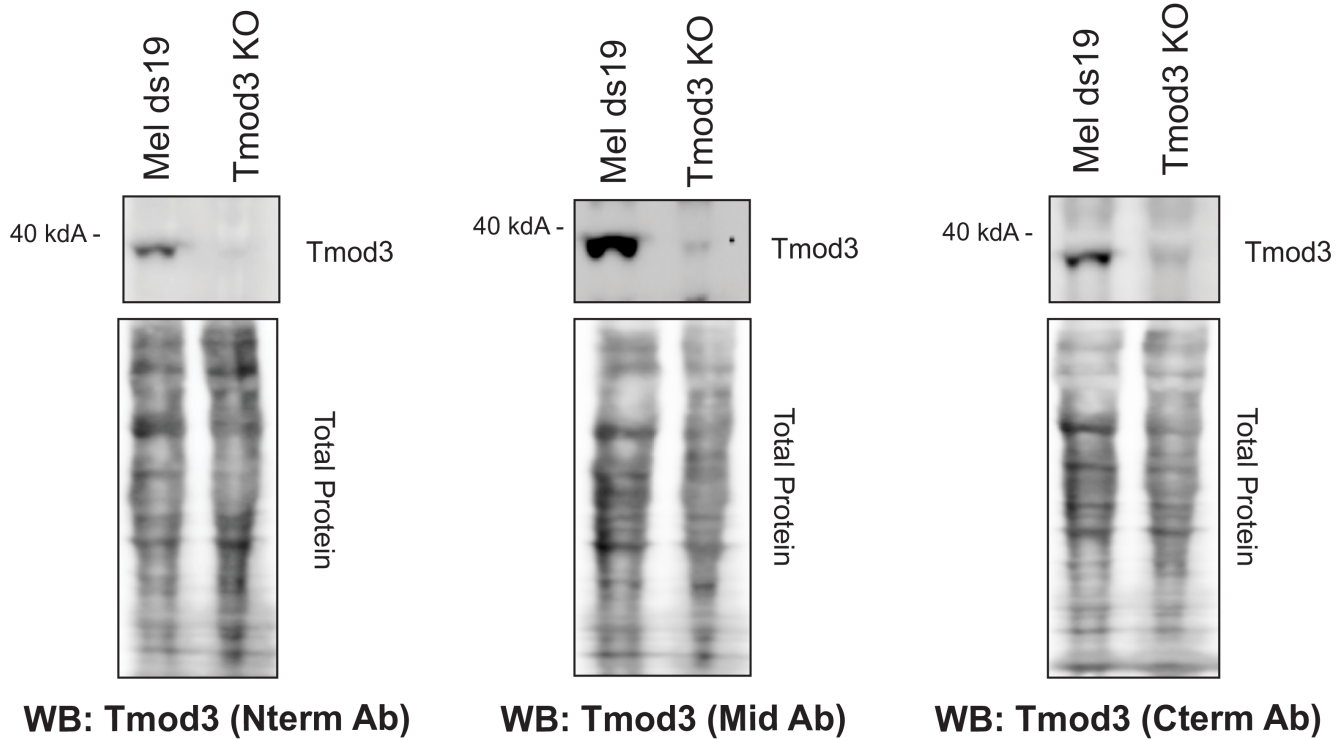
GPFDRELLSYLEKQALEHKDRDDYVPYTGEKKGKIFIPKQKPAQTLTEETISLDPELEEAL T

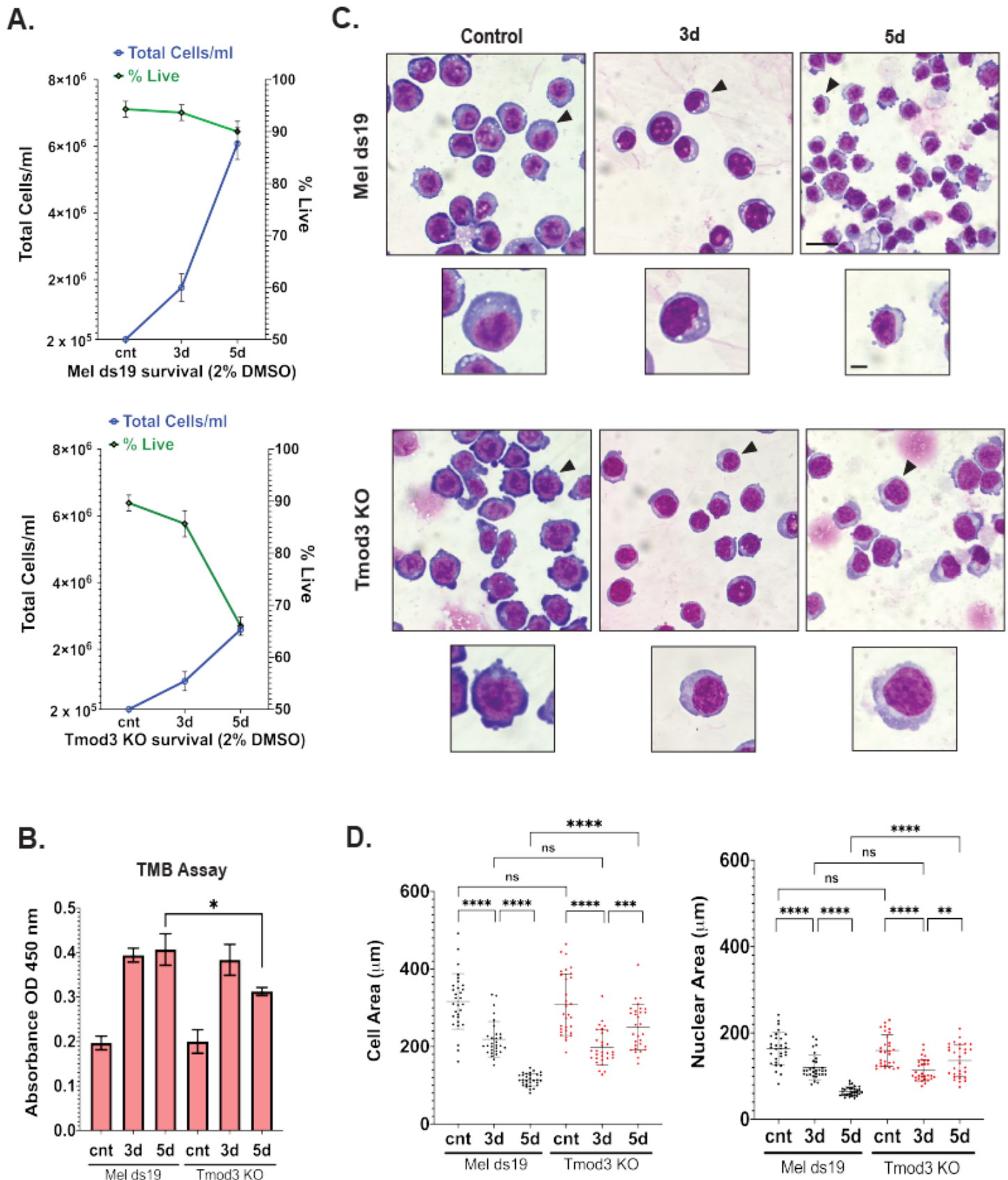
SASDELCDLAAILGMHNLIADTPFCVDLGSSNGVNQERFPNVVKGEKILPVFDEPPNPTN T

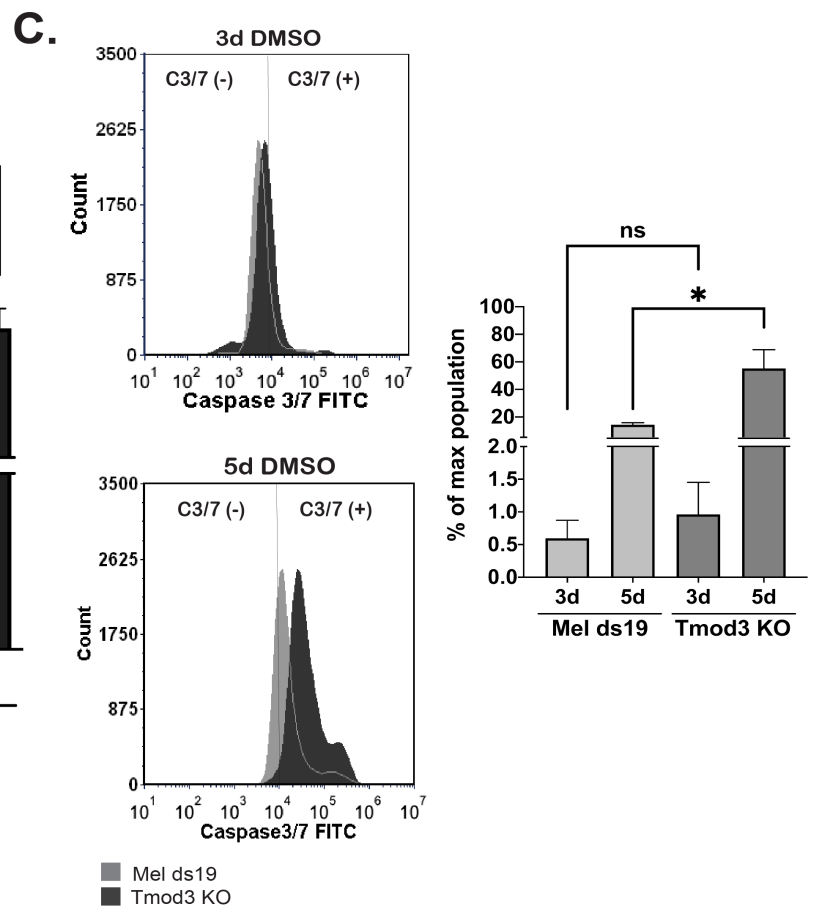
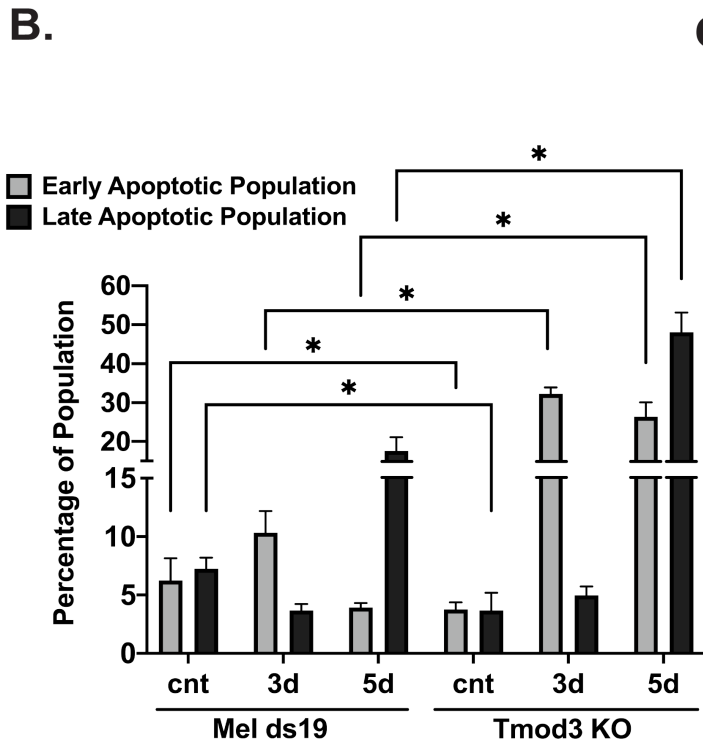
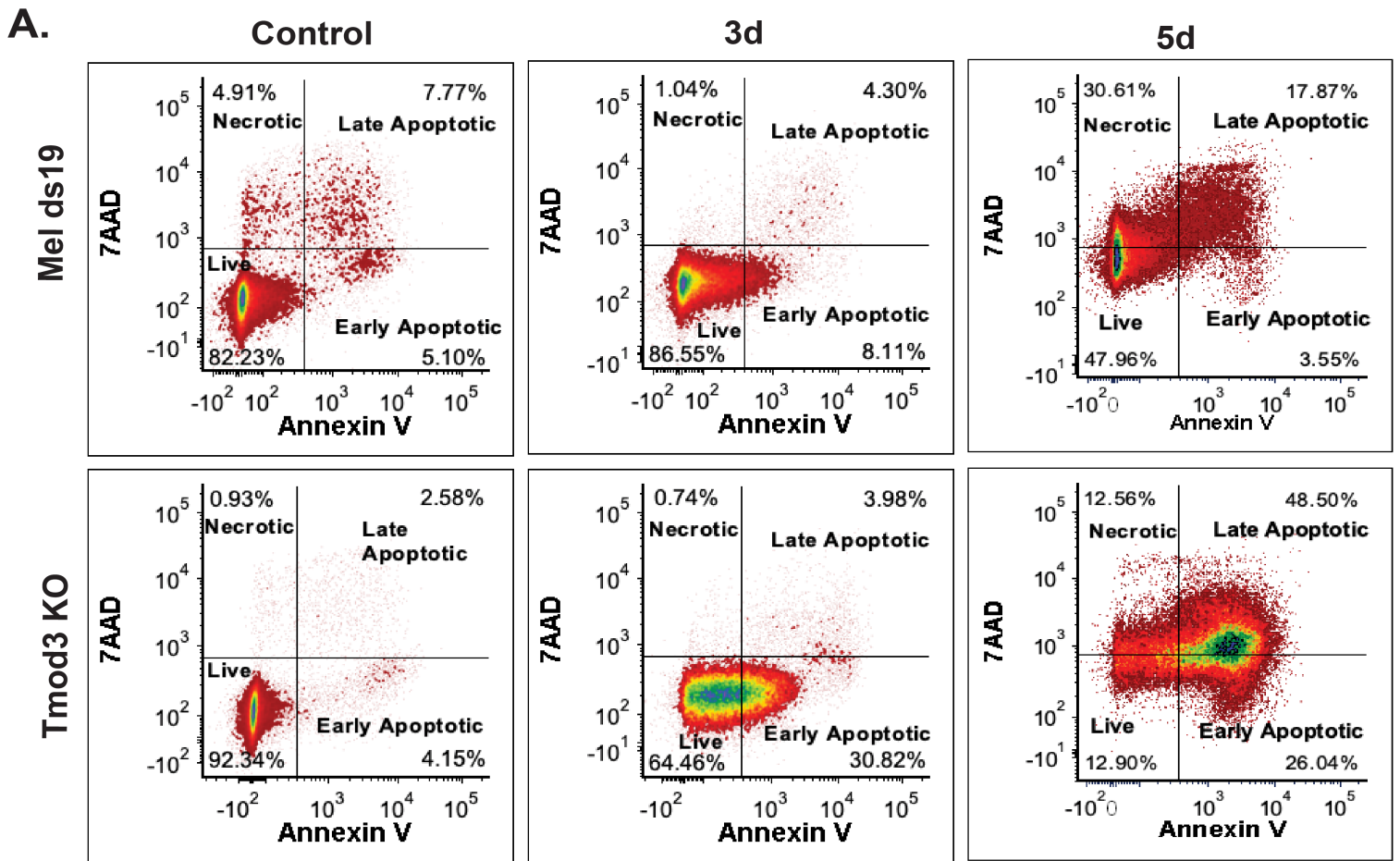
VEESLKRIRENDARLVEVNLNNIKNIPIPTLKDFAKTLEANTHVKHFSLAATRSNDPVAVAF A

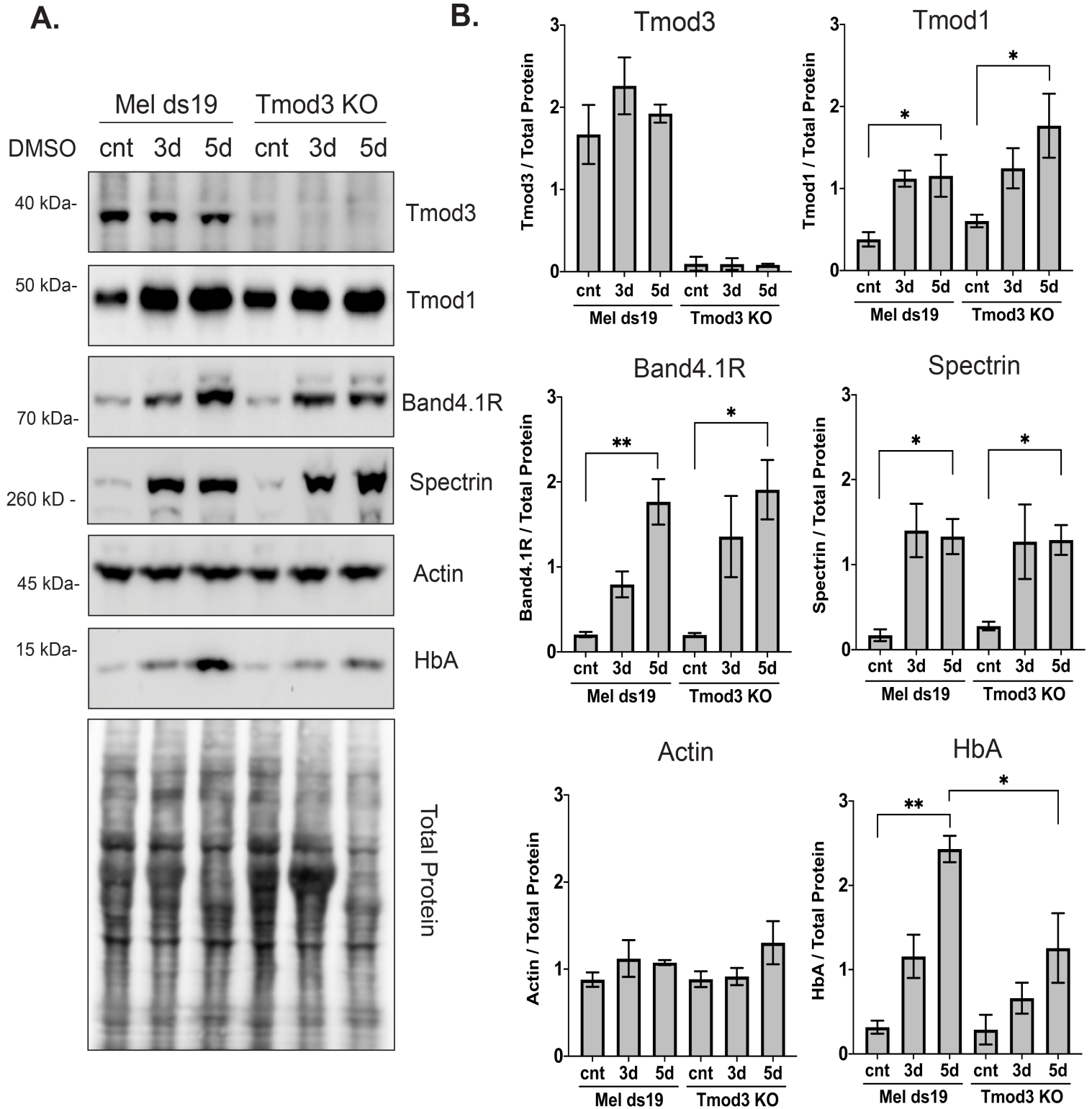
DMLKVNKTLKSLNMESNFITGAGVLALIDALRDNETLMELKIDNQRQQLGTSVELEMAKML

EENTNILKFGYQFTQQGPRTRAANAITKNNDLVRKRRIEGDHQ Tmod3 (Cterm Ab) △

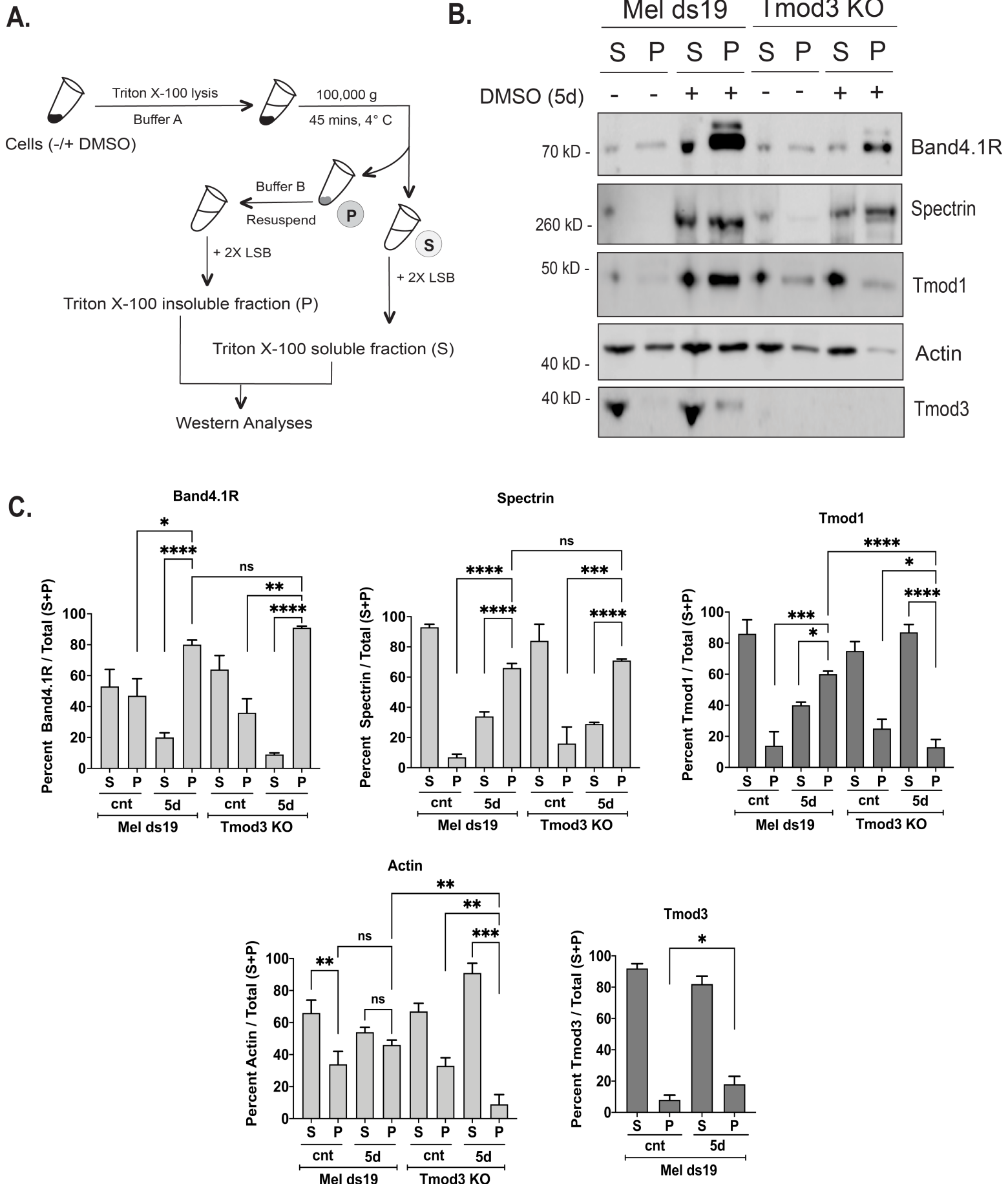


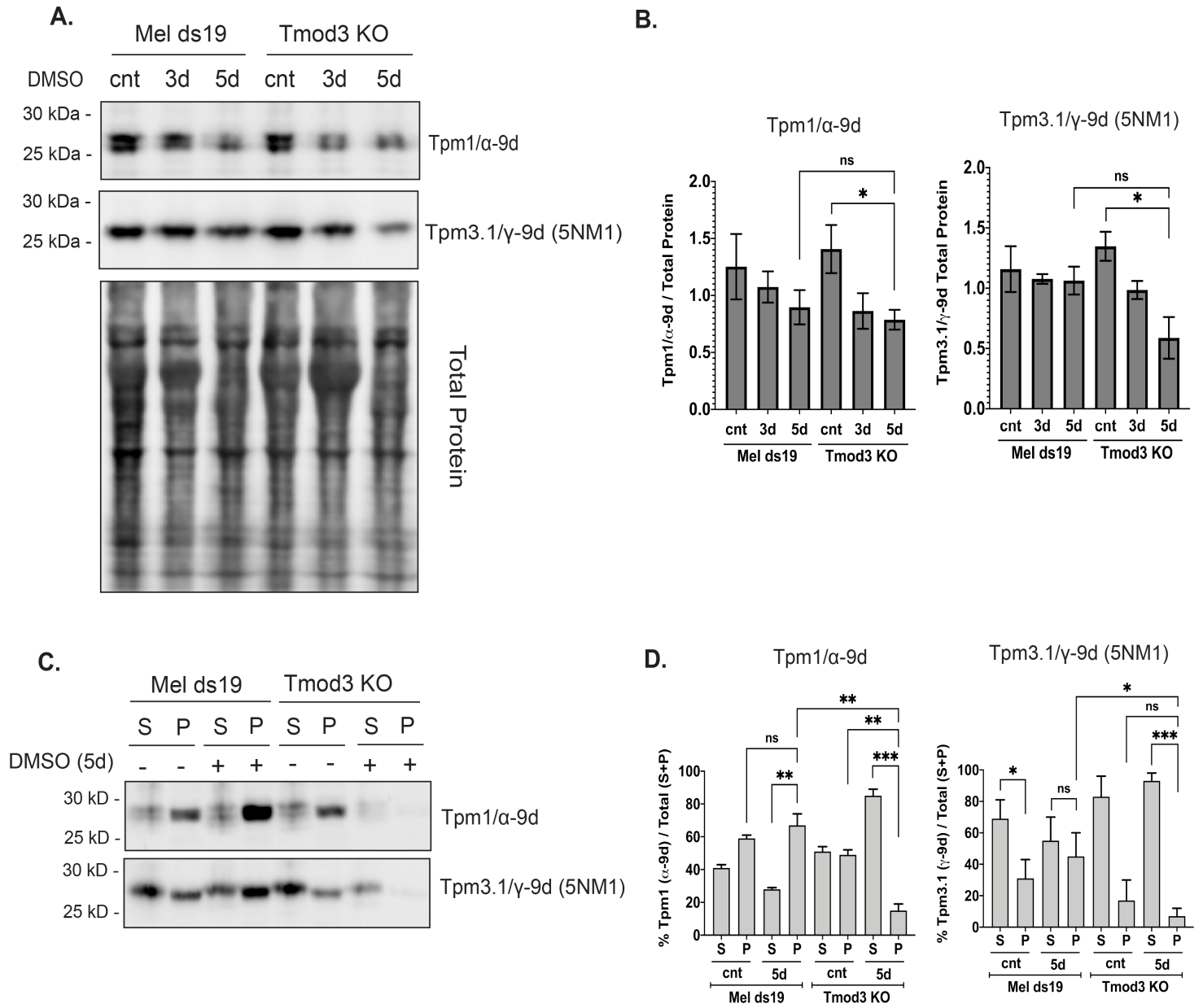






# Figure 5





**Table 1**

List of primers for guide RNA insertion in psp-Cas9-GFP Vector (PX458)		
Guide ID	Sample ID	sgRNA primer
Guide – sgRNA1	Tmod3_sg1_Top	5’-CACCGTTCGCCTCTTGCGCACTGTG-3’
	Tmod3_sg1_Bottom	5’-AAACCACAGTGCGCAAGAGGCGAAC-3’
Guide – sgRNA2	Tmod3_sg2_Top	5’-CACCATTGTTCTTCGTTATCGCGT-3’
	Tmod3_sg2_Bottom	5’-AAACACGCGATAACGAAGAACAATC-3’
Guide – sgRNA3	Tmod3_sg3_Top	5’-CACCAATTCGCCTCTTGCGCACTG-3’
	Tmod3_sg3_Bottom	5’-AAACCAGTGCGCAAGAGGCGAATTC-3’
List of primers for off-target analysis		
Chromosome, Position	Primer ID	Primer Sequence
Chr5, 24,699,170	Chr5 Off FWD	5’ -GTGCTGAGCCTGTGCCTTGC- 3’
Chr5, 24,699,610	Chr5 Off REV	5’ -GCGCCAGAACTGTTGTTTCCTC- 3’
Chr6, 144,820,280	Chr6 Off FWD	5’ -GAGGTCAGTCAGGCTACGCTCC- 3’
Chr6, 144,820,700	Chr6 Off REV	5’ -GAAAGGGCGTGAGTTGGTCGC- 3’

## Supplemental Figure Legends

**Supplementary Figure S1. FACS sorting for *Tmod3* knockout cells.** (A) Flow cytometry panels showing FACS-sorting for Mel ds19 cells electroporated with the plasmid (pSpCas9(BB)-2A-GFP, PX458) expressing sgDNA directed to exon 9b of *Tmod3* gene. A control vector lacking GFP was used to gate for non-GFP fluorescing cells (SSC-A (side scatter-area) vs GFP). The GFP positive cells post-sorting were expanded for clonal selection and screened for loss of *Tmod3* via western blotting (data not shown). The selected clone was passaged five times to ensure loss of Cas9-GFP from the cell line and checked via the aforementioned FACS (gating) methodology to ascertain removal of Cas9 from the cells. Cell sorting was carried out on a BD FACSAria Fusion High Speed Cell Sorter. (B) Genomic DNA from unedited Mel ds19 and *Tmod3* knockout cells was used to PCR amplify the guide RNA binding site with primers flanking the region. The PCR products were sequenced to reveal the cleavage region in the knockout clone. Sequencing chromatograms are shown for both Mel ds19 and *Tmod3* knockout cells. Comparison of the bottom with the top panel shows that the *Tmod3* knockout has missing bases, which leads to total protein loss (see Figure 1B). The guide RNA binding sequence and the PAM site are shown along with the cleavage site.

**Supplementary Figure S2. Off-target analyses for sgRNA2 in Mel ds19 and *Tmod3* knockout cells.** (A) Predicted off-target sites for the guide sgRNA2 was obtained from the guide RNA design program - <https://chopchop.cbu.uib.no/> and the coordinates (Chromosome 5 and Chromosome 6) were used to find respective sequence information in the UCSC genome browser (<https://genome.ucsc.edu/>). A ~400 bp region was amplified from Mel ds19 and *Tmod3* KO genomic DNA using primers flanking the site of interest and analyzed via Sanger sequencing. (B) Sequencing chromatograms for Mel ds19 and *Tmod3* KO are shown for both Chromosome 5 and Chromosome 6

predicted off-target sites. No difference between edited and unedited samples were observed in the sequence information, indicative of no off-target effects for the sgRNA2 expression in the knockout.

**Supplementary Figure S3. CD71 expression during erythroid differentiation is similar in Mel**

**ds19 and in Tmod3 knockout cells.** (A) Experimental design for detecting surface and internal CD71 levels via flow cytometry. Cells were stained with anti-CD71 PE antibody followed by fixing and permeabilization using fix and perm kit (according to manufacturer's instructions, Thermo Fisher), and thereafter the internal CD71 protein was labeled with anti-CD71 APC antibody. Cells were subsequently analyzed by flow cytometry using a BD Accuri C6 flow cytometer. (B,C) FACS dot plots for Mel ds19 and *Tmod3* KO cell lines showing fluorescence intensity of surface CD71 PE (upper panels, B) or internal CD71 APC (lower panels, C) represented as percentage of population P1 (CD71 low) and P2 (CD71 high) versus side scatter (SSC-A). The vertical line marker (at  $\sim 10^3 - 10^4$  MFI) separates CD71 unstained and CD71 stained populations. Percentage of populations – P1 (CD71 low) and P2 (CD71 high) were graphed as a percentage of P1+P2 population for Mel ds19 and *Tmod3* knockout cells at undifferentiated (cnt), 3d and 5d DMSO timepoints. Values represent means and error bars  $\pm$  SD (n=5). Dot plots were generated using FCS Express 7 research (De Novo™ Software).

**Supplementary Figure S4. Isotype control for CD71 PE and CD71 APC.** (A) Experimental setup

for isotype control for PE and APC antibodies. Mel ds19 cells were either grown with or without 2% DMSO and stained as indicated – Set1 (unstained, isotype control PE and CD71 PE surface) or Set 2 - fixed and perm (unstained, Isotype control PE + Isotype control APC, CD71 PE surface + cytoplasmic CD71 APC). (B) Histograms indicative of FACS profiles for Set 1 and Set 2 are shown for control and DMSO-treated Mel ds19 cells. The isotype control PE is indicative of background from the IgG1 while isotype control APC is indicative of background from IgG2. Both CD71 PE and

CD71 APC signals are higher compared to background, thus representing the fluorescence signals from the respective CD71 surface receptor expression or CD71 internal expression. Cells were analyzed on a FACS Aria Fusion and data was analyzed with FCS Express 7.

**Supplementary Figure S5. Nuclear to cell area ratiometric measurements for Mel ds19 and Tmod3 knockout.** Giemsa-stained Mel ds19 and Tmod3 KO cells (treated or untreated with 2% DMSO) were analyzed for nuclear and cell area. The ratio of nuclear to cell area was plotted for ~30 cells from each condition; data shown is representative of three independent experiments. Values represent means and error bars  $\pm$  SD (n=30). Paired student's T-tests were used to determine significance. ns – not significant, \*  $p \leq 0.05$ , \*\*  $p \leq 0.01$ , \*\*\*  $p \leq 0.001$ .

**Supplementary Figure S6. Caspase 3/7 expression is higher in Tmod3 knockout during erythroid differentiation compared to Mel ds19.** (A) Experimental design for Caspase3/7 assay. Cells growing with or without DMSO were washed 2X with PBS before incubating with the CellEvent™ Caspase3/7 green detection reagent followed by SYTOX-7AAD (as a live/dead stain). Caspase3/7 was detected via excitation with a 488 nm laser in the FITC channel on a BD Accuri C6 flow cytometer. Cells gated for 7AAD negative (live; parent gate, data not shown) were used to gate for the Caspase3/7 positive signal. (B) Unstained Mel ds19 cells were used to establish the gating strategy for detection of Caspase3/7 in the FITC channel. A representative flow cytometry panel is shown [SSC (side scatter) vs Caspase 3/7 FITC]. The unstained cell population (99.52%) is shown in the lower left quadrant of the flow panel. (C) Cells stained with Cell Event™ Caspase 3/7 dye were analyzed via flow cytometry and detected as fluorescence in the FITC channel for Mel ds19 and Tmod3 knockout cells (undifferentiated/control, 3d and 5d DMSO). Percentage fluorescence intensity is denoted in each gate on lower left (C3/7-) and lower right (C3/7+). The cell count events

are indicated by the fluorescence intensity (color) scale shown in the count legend at the bottom. All experiments were conducted on BD Accuri C6 flow cytometer and in triplicates (N=3).

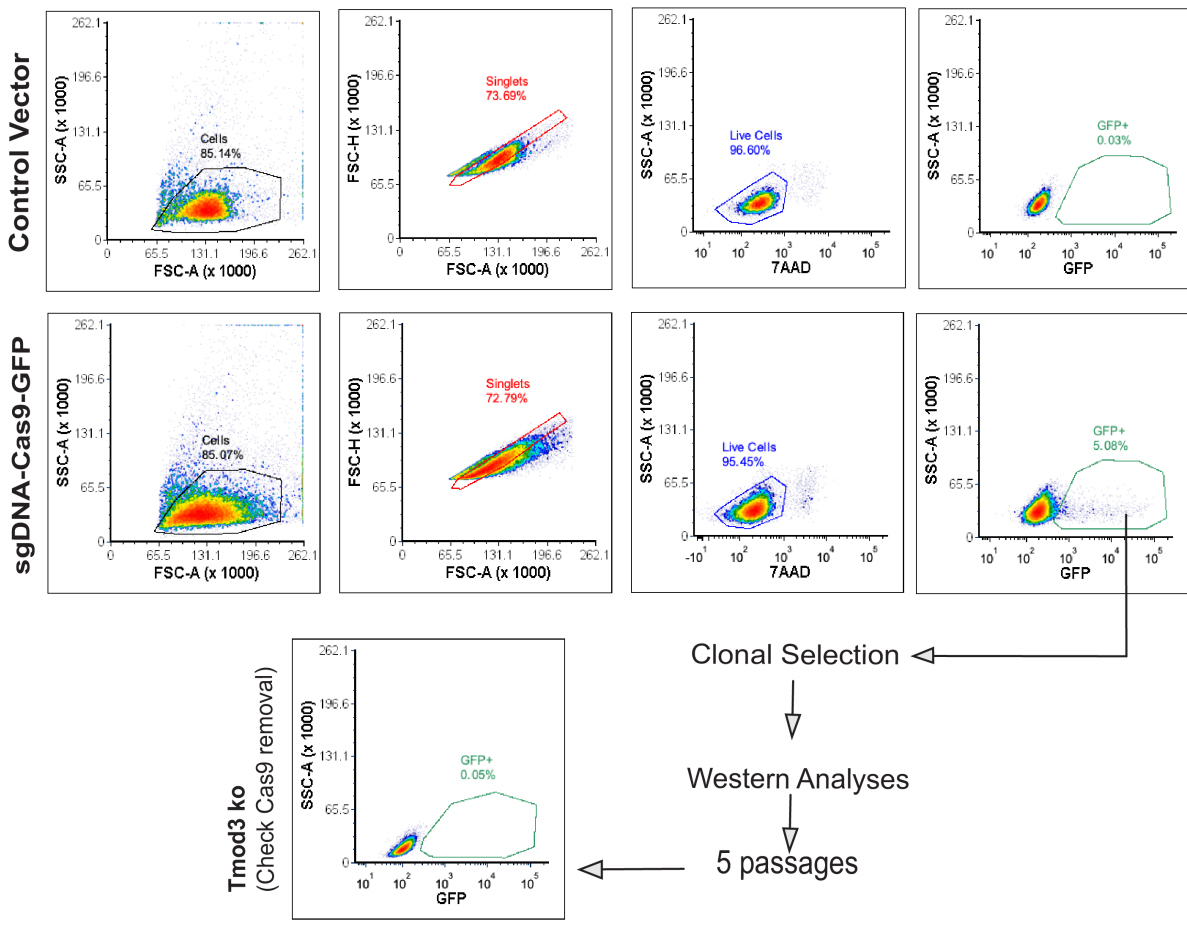
**Supplementary Figure S7. Cell cycle analysis for Mel ds19 and *Tmod3* knockout during erythroid differentiation.**

(A) Representative flow cytometry panels for Mel ds19 and *Tmod3* knockout cells at control or 5d DMSO timepoints. Cells were stained with propidium iodide (PI) and analyzed on a BD FACS Aria Fusion for cell cycle characterization. Top (row) panels show SSC (side scatter) plotted against FSC (forward scatter) and the gate P1 represents  $SSC^{low}FSC^{high}$ . Third (row) panels – Single Cell Gate represents P1 cells gated for single populations and represented as the P2 gate. In the third row of panels, the 2N vs 4N populations are shown as PI versus SSC-H (side scatter height) with gates 2N and 4N for each subpopulation. For 5d DMSO, Mel ds19 and *Tmod3* KO panels, the 2N population (G1 cells) is sub-gated into two populations – G1+ and G1++ where the latter population indicates cells with greater granularity (internal complexity). The bottom (last row) panels denote histograms for multicycle analysis to model cell cycle stages (%G1, %S, %G2) and are represented as cell counts versus the PI fluorescence. The analysis was conducted on FCS express 7 research (De Novo Software) using the multicycle analysis plugin. (B) For differentiating (5d) Mel ds19 and *Tmod3* knockout cells, the gates on the 2N population (G1+, G1++) were graphed to assess differences in granularity. The percentage of cells in each population was graphed on the Y axes. The *Tmod3* KO G1++ gate indicates that the knockout cells are ~5% more granular than the parental line. (C) Cell cycle parameters (%G1, %S, %G2) from the multicycle analysis generated percent population values for each cell cycle stage. The percentages are shown in the graph with percentage of max population on the Y-axes for control (undifferentiated) and 5d (differentiating) timepoints for respective cell lines. No significant differences were observed between the Mel ds19 and the *Tmod3* knockout cells. Values represent means, with error bars  $\pm$  SD (n=3).

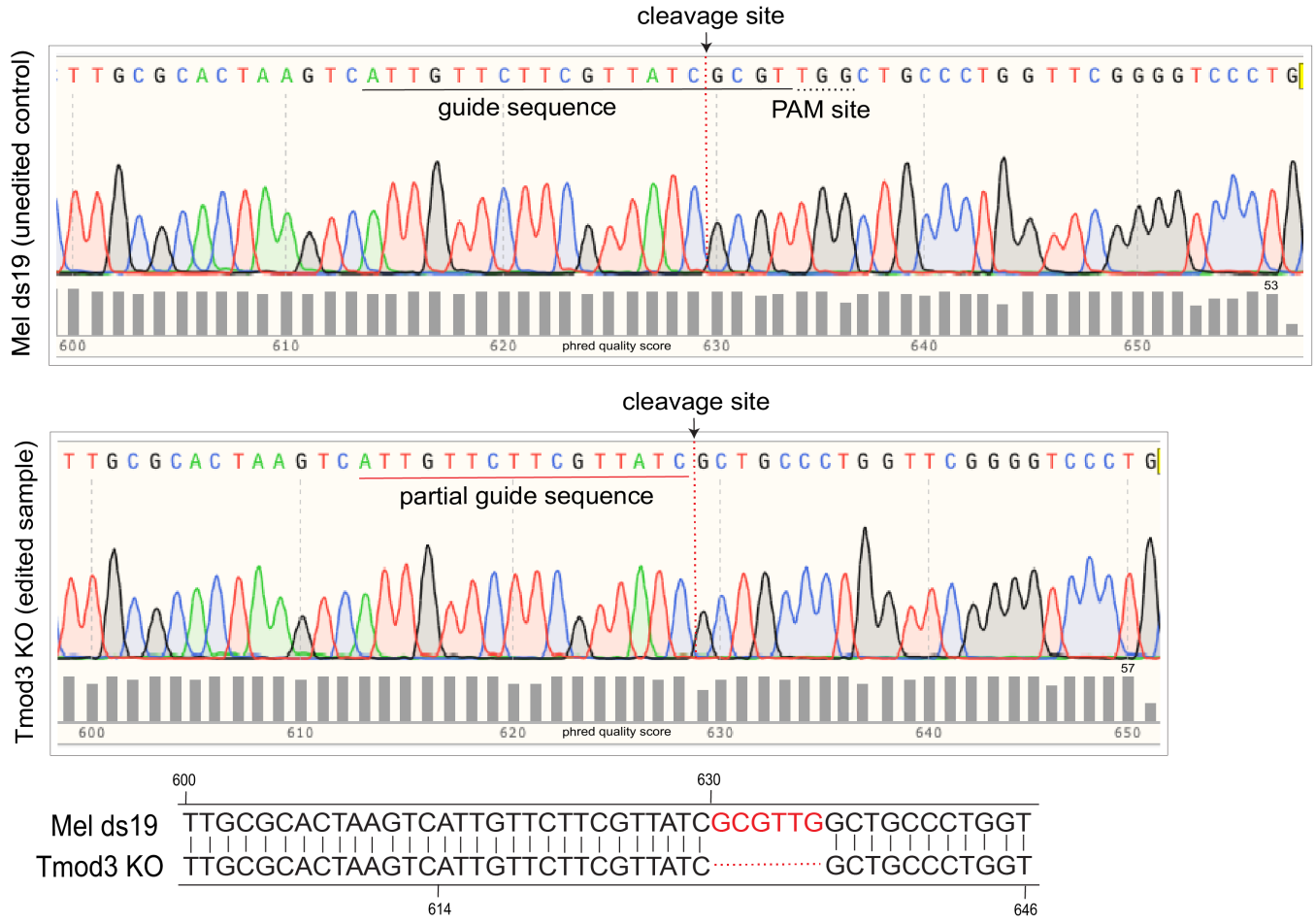
**Supplementary Figure S8. Tropomyosin protein levels in Mel ds19 cells.** (A) Three different Tpm antibodies were used to analyze the expression of these proteins in Mel ds19 cells. Total cell lysates for Mel ds19 cells were prepared as mentioned before (Materials and Methods) and immunoblotted for Tpm 1/ $\alpha$ -9d, Tpm 3.1/ $\gamma$ -9d (5NM1) and Tpm 4/Tm4. Total protein was analyzed via Revert<sup>TM</sup> stain. Based on the expression levels, only Tpm 1/ $\alpha$ -9d and Tpm 3.1/ $\gamma$ -9d (5NM1) were further analyzed for Tmod3 loss in this study. Three independent replicates are shown.

**Supplementary Figure S9. Fractionation in Mel and Tmod3 KO cells** (A, B) Total proteins in S and P fractions in Triton X-100 fractionation assays. Samples from the Triton X-100 fractionation assay denoted as Triton X-100 soluble (S) versus insoluble (P) fractions, were analyzed for total protein prior to blocking and antibody incubation. Post-transfer, the PVDF membranes were incubated in Revert<sup>TM</sup> total protein stain (LiCoR) and visualized in the 700 nm channel using a Biorad ChemiDoc. A representative stained membrane is shown corresponding to samples displayed in Figure 5b (A) or Figure 6c (B). (C) The distribution of actin in Tx-100 in the S and P fractions reflects G-actin and F-actin, respectively. Using the actin depolymerizing drug, Latrunculin B, or actin polymerizing drug, Jasplakinolide, we determined that F-actin preferentially fractionates with the Tx-100 insoluble membrane skeleton fraction. Treatment of growing Mel ds19 cells with 0.5  $\mu$ M Latrunculin B for 30 mins shifts the actin pool into the soluble fraction (S) indicative of increased G-actin, as expected. By contrast, treatment of cells with 0.5  $\mu$ M Jasplakinolide shifts the actin pool into the Tx-100 insoluble membrane skeleton fraction, indicating increased actin polymerization (F-actin). Thus, the S and P fractions measured in this assay reflect the relative proportion of actin that is present as G-actin or F-actin, respectively, in the Mel cells.

A.



B.



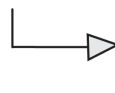
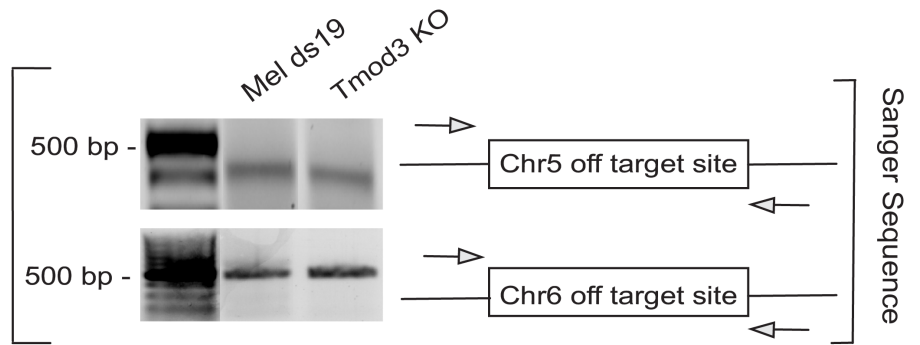
## Figure S2

A.

## sgRNA2 Predicted Off Target Site

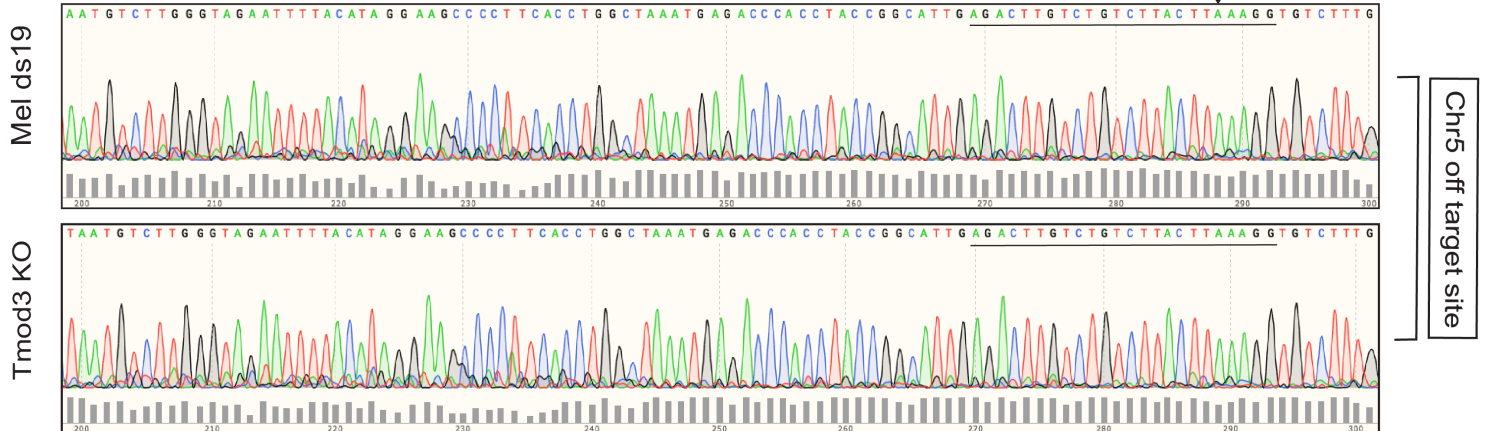
Chr5 (position - 24,699,170)

Chr6 (position - 144,820,385)

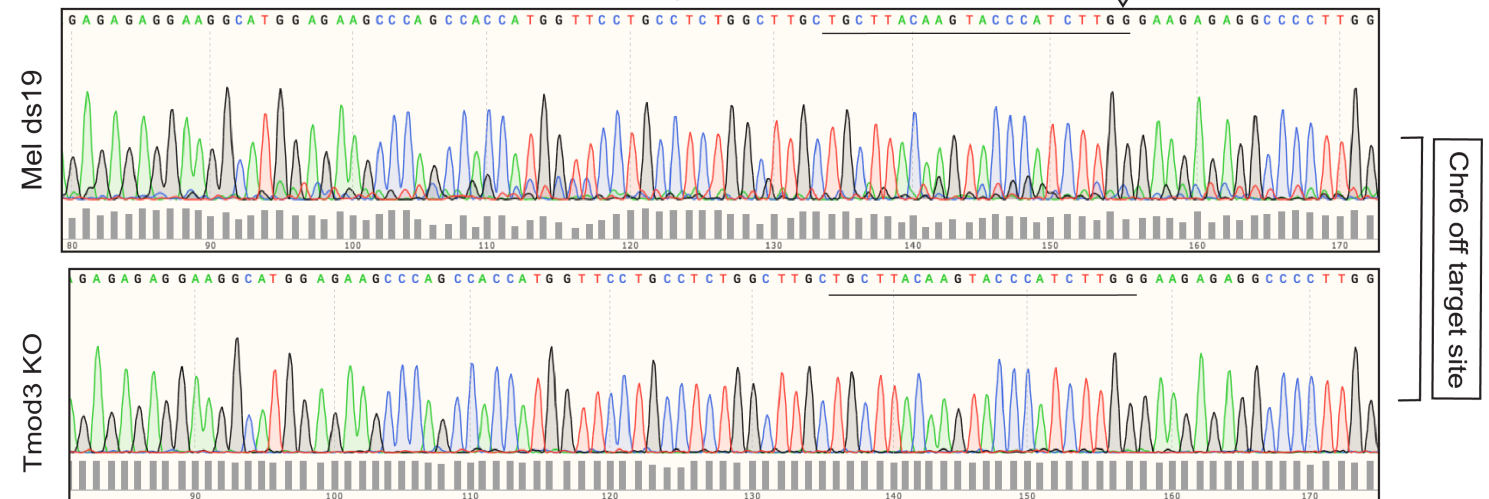
 UCSC genome browser


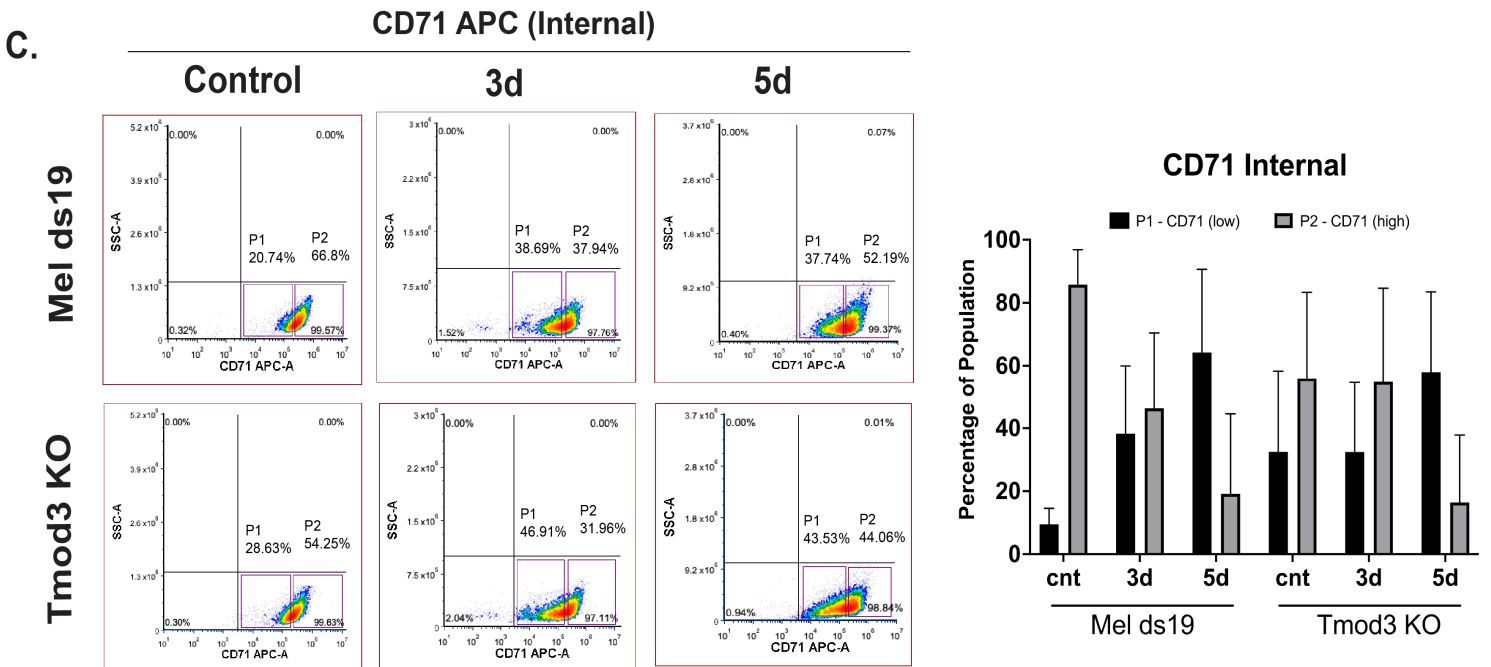
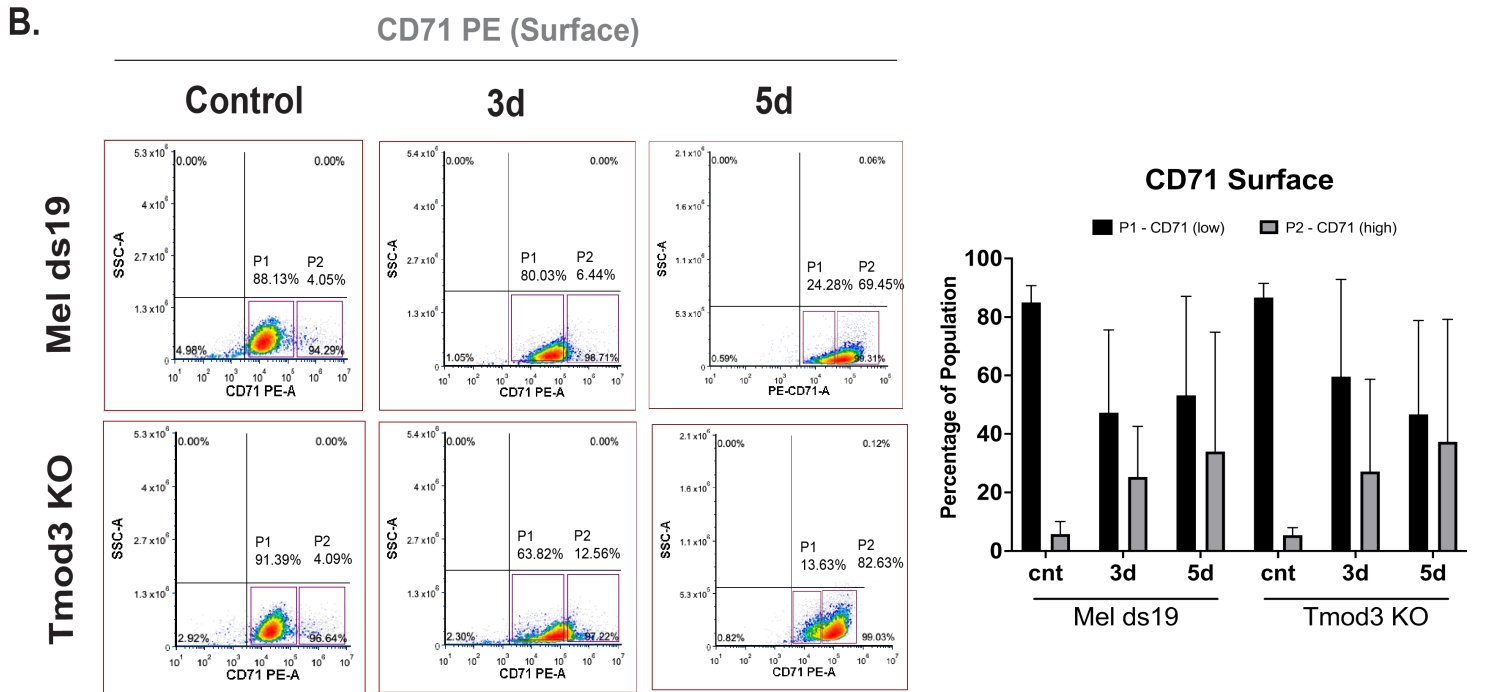
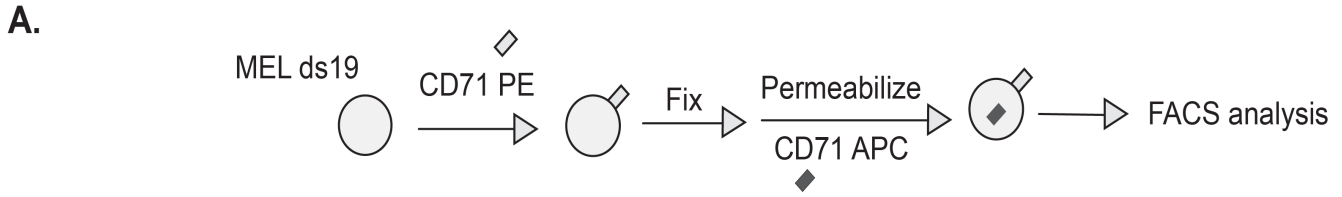
B.

predicted guide binding with mismatches



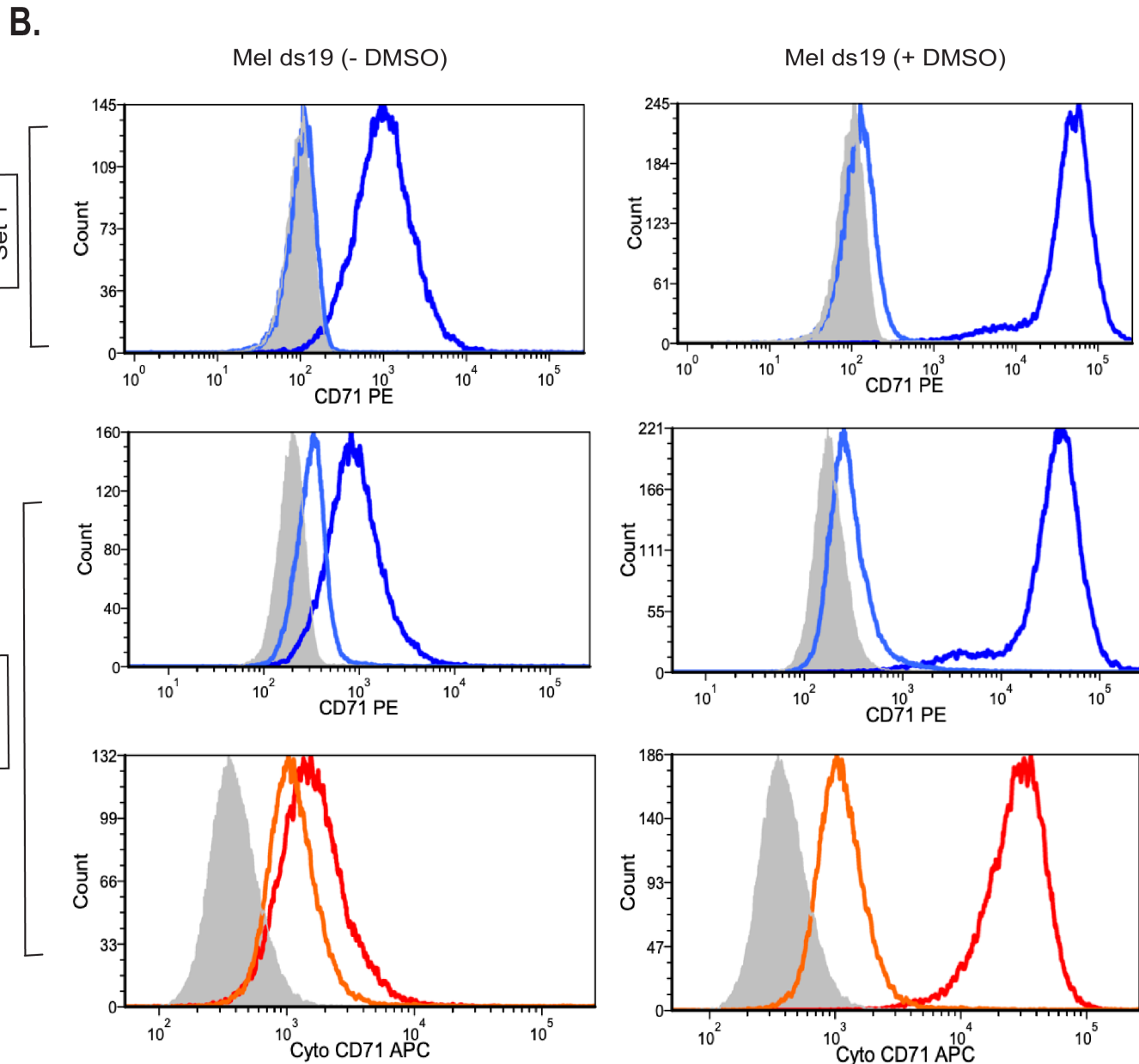
predicted guide binding with mismatches





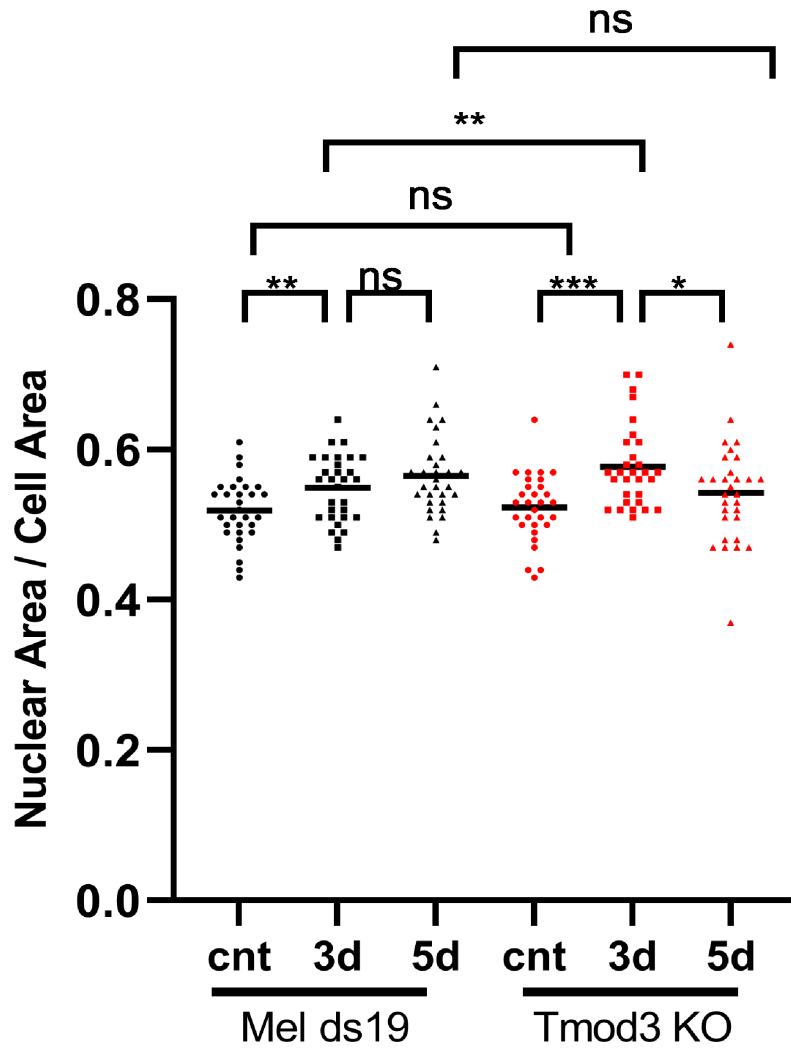
**A.**

<p><b>Set 1</b>                  Unstained                  Isotype Control PE                  CD71 PE surface</p>	<p><b>Set 2</b>                  Unstained (fix &amp; perm)                  Isotype Control PE + cytoplasmic Isotype Control APC (fix &amp; perm)                  CD71 PE surface (fix &amp; perm) + cytoplasmic CD71 APC (fix &amp; perm)</p>
---	--

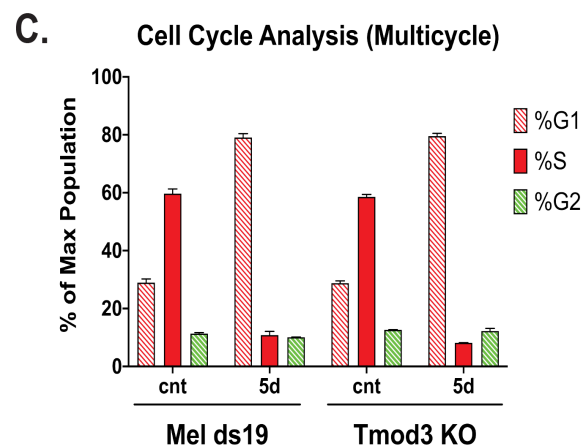
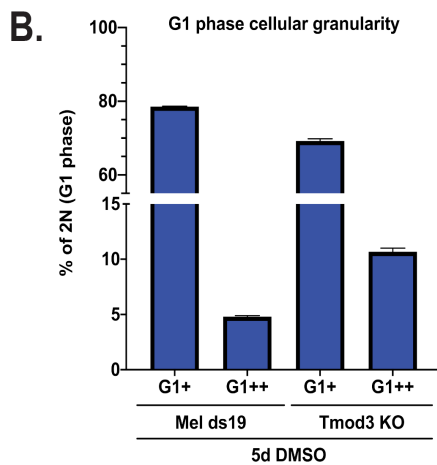
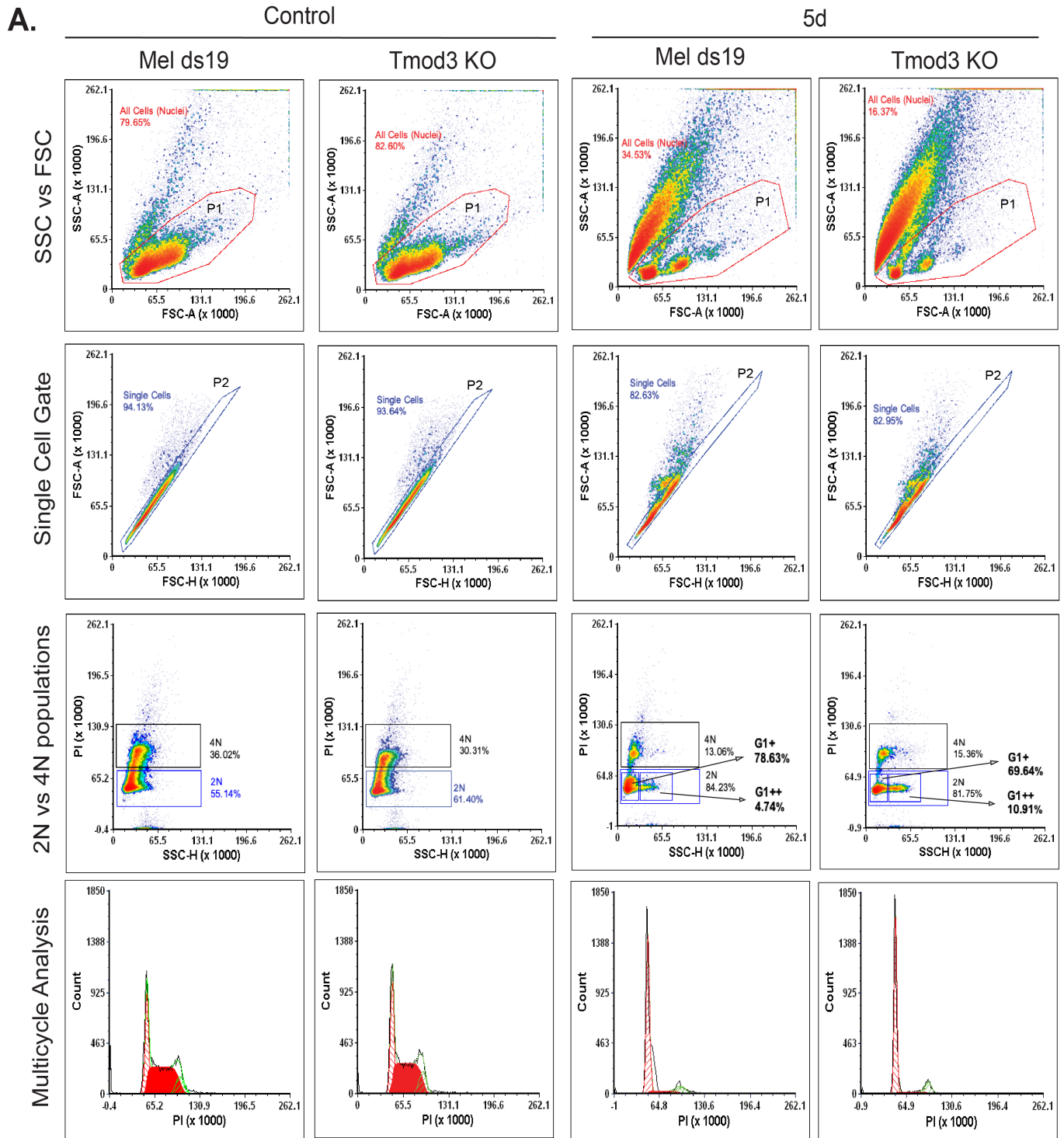


Unstained	Isotype Control APC
Isotype Control PE	CD 71 APC
CD 71 PE	

Figure S5

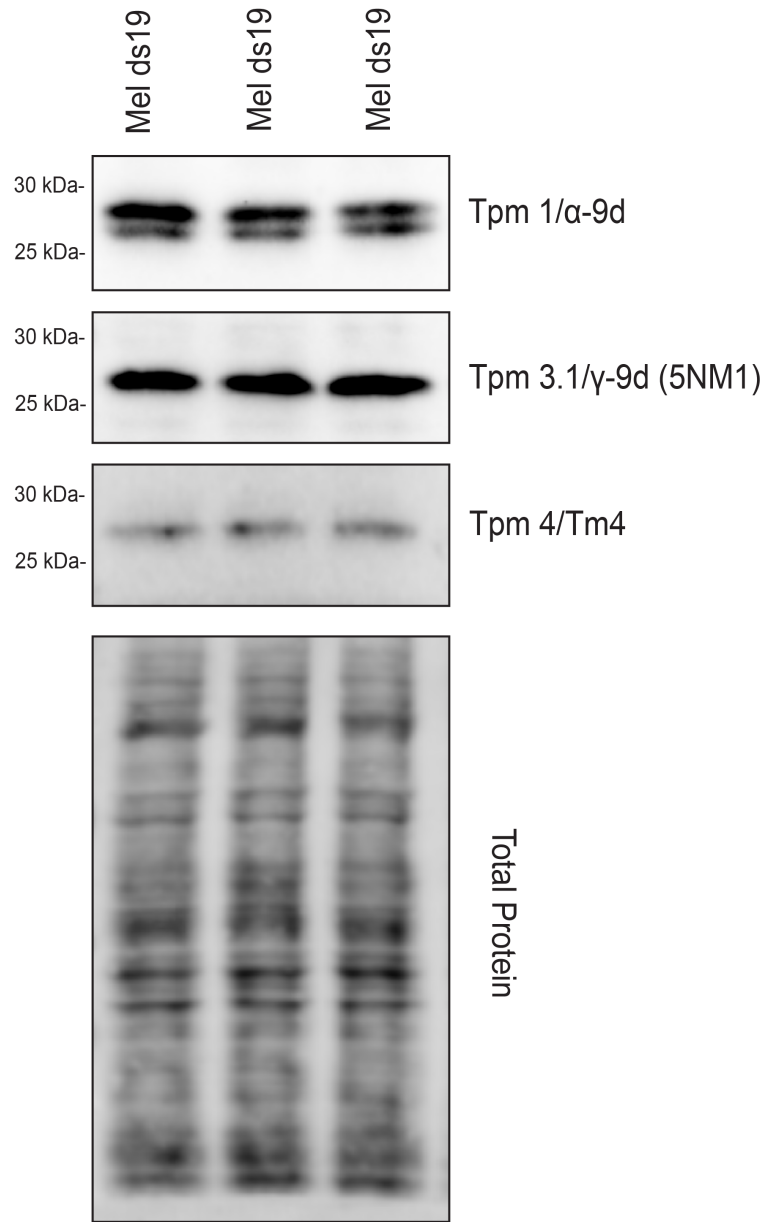






# Figure S8

**A.**

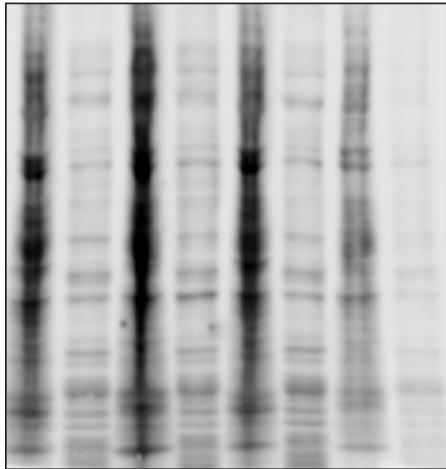


## Figure S9

**A.**

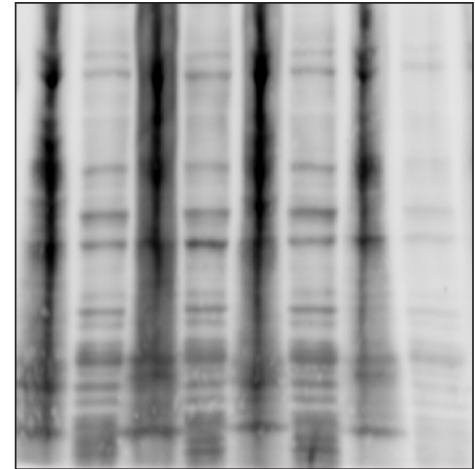
Total Protein per sample in Figure 5b

	Mel ds19				Tmod3 KO			
	S	P	S	P	S	P	S	P
DMSO (5d)	-	-	+	+	-	-	+	+

**B.**

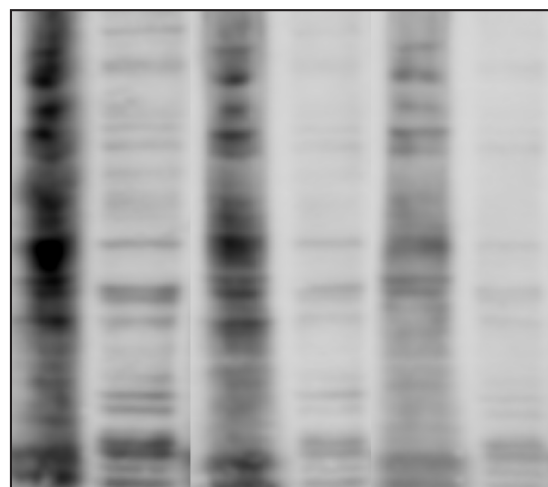
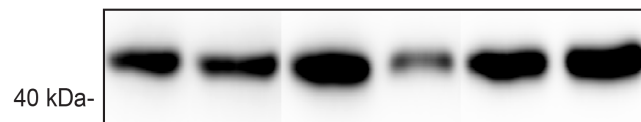
Total Protein per sample in Figure 6c

	Mel ds19				Tmod3 KO			
	S	P	S	P	S	P	S	P
DMSO (5d)	-	-	+	+	-	-	+	+

**C.**

Mel ds19

	S		P		S		P	
0.5 $\mu$ M LatB	-	-	+	+	-	-	-	-
0.5 $\mu$ M Jasp	-	-	-	-	+	+	+	+



**Supplemental Table 1**

Table S1		
Reagent/Resource	Source	Catalog No.
Plasmids; Bacterial strains		
pSp-Cas9(BB)-2A-GFP (PX458)	Addgene	48138
DH5 $\alpha$ competent cells	Thermo Fisher	18258012
Plasmid Miniprep Kit	Qiagen	12943
Chemicals/equipment		
DMEM culture media	Fisher Scientific	10-13-CV
Fetal Bovine Serum	GenClone	25-550H
Pen/Strep	Gibco	15140-122
BbsI	New England Biolabs	R0539S
T4 DNA ligase	New England Biolabs	M0202S
T4 Polynucleotide kinase	New England Biolabs	M0201S
Trypan Blue	Millipore Sigma	15250061
7AAD	Biolegend	420403
Cytofunnel	Thermo Fisher	59-910-40
Giemsa Stain	Sigma-Aldrich	GS500
TMB Substrate Kit	Pierce (Thermo Fisher)	34021
BCA Assay Kit	Thermo Fisher	23250
DMSO	Millipore Sigma	472301
Annexin V binding buffer (5X)	BioLegend	V13246
Annexin V Brilliant Violet 421	BioLegend	640924
CellEvent <sup>TM</sup> Caspase 3/7	Thermo Fisher	C10423
Propidium Iodide	Sigma-Aldrich	P-4170
IGEPAL CA-630	Sigma-Aldrich	I8896
Halt <sup>TM</sup> Protease Inhibitor Cocktail	Thermo Fisher	78429
Halt <sup>TM</sup> Phosphatase Inhibitor Cocktail	Thermo Fisher	78420
Cytochalasin D	Thermo Fisher	PHZ1063
RNase A	Sigma-Aldrich	R-5000
Triton X-100	Sigma-Aldrich	X-100
2X Laemmli Sample Buffer	Biorad	1610737
Novex Tris-glycine SDS gel (4-12%)	Thermo Fisher	XP04125BOX
Novex Tris-glycine SDS gel (4-20%)	Thermo Fisher	XP04205BOX
PVDF Immobilon Transfer Membrane	Millipore Sigma	IPFL00010
Fix and Perm Cell Permeabilization kit	Thermo Fisher	GAS003
Revert Total Protein Stain	LiCoR	926-11011
Antibodies		
Tmod3 (Nterm Ab, Chicken Polyclonal, affinity purified), AB – pAB4 SC1056 peptide	Genscript	Custom-made R158181-5
Tmod3 (Cterm Ab, Chicken Polyclonal, affinity purified), B – pAB1 SC1056 peptide	Genscript	Custom-made R151818-2
Tmod3 (Mid Ab, Rabbit Polyclonal)	Aviva	ARP55078_P050
Tmod1 (Rabbit polyclonal, affinity purified,	Fowler,1990. J. Cell	Custom-made

R1749 Bleed3A, Tmod3 pre-cleared)	Biol.	
Band 4.1R (Rabbit Polyclonal, affinity purified)	Cathy Korsgren & Sam Lux, Harvard Medical School, Boston MA	Gift
a1,b1-spectrin (Rabbit polyclonal, affinity purified)	Cathy Korsgren & Sam Lux, Harvard Medical School, Boston, MA	Gift
Pan-Actin (C4; Mouse Monoclonal)	EMD Millipore Sigma	MAB1501
Hemoglobin A	Santa Cruz	sc-514378
Tpm1/ $\alpha$ -9d (Tpm2,3,5a,5b,6; Sheep Polyclonal)	EMD Millipore Sigma	AB5441
Tpm3.1/ $\gamma$ -9d (5NM1, Sheep Polyclonal)	EMD Millipore Sigma	AB5447
Tpm4.1/Tm4 (Rabbit Polyclonal)	EMD Millipore Sigma	AB5449
PE Rat Anti-mouse CD71 (Clone C2)	BD Biosciences	561937
APC Rat Anti-mouse CD71	Biolegend	113819
Fc Block	BD Biosciences	553142
PE Rat IgG1, k Isotype Control	BD Pharmigen	553925
APC Rat IgG2a, k Isotype Control	Biolegend	400511
IRDye <sup>®</sup> 800CW Donkey anti-Goat IgG (Secondary Ab) - used with anti-Sheep Primary	LiCoR	926-32214
IRDye <sup>®</sup> 680RD Donkey anti-Goat IgG (Secondary Ab) - used with anti-Sheep Primary	LiCoR	926-68074
IRDye <sup>®</sup> 800CW Donkey anti-Rabbit IgG (Secondary Ab)	LiCoR	926-32213
IRDye <sup>®</sup> 800CW Donkey anti-Mouse IgG (Secondary Ab)	LiCoR	926-32212
IRDye <sup>®</sup> 680RD Donkey anti-Rabbit (Secondary Ab)	LiCoR	926-68073
IRDye <sup>®</sup> 680RD Donkey anti-Mouse IgG (Secondary Ab)	LiCoR	926-68072